frontiers | Frontiers in Environmental Science

TYPE Original Research
PUBLISHED 14 February 2024
DOI 10.3389/fenvs.2024.1360453

OPEN ACCESS

EDITED BY
Huizhong Shen,
Southern University of Science and Technology, China

REVIEWED BY
Jinghao Zhai,
Southern University of Science and Technology, China
Yilin Chen,
Peking University, China
Dimitris G Kaskaoutis,
National Observatory of Athens, Greece

*CORRESPONDENCE
Jiao Tang,
tangjiao@gig.ac.cn
Gan Zhang,
zhanggan@gig.ac.cn

RECEIVED 23 December 2023
ACCEPTED 26 January 2024
PUBLISHED 14 February 2024

CITATION
Zhang B, Tang J, Geng X, Mo Y, Zhao S, Zhong G, Li J and Zhang G (2024), Seasonal changes in water-soluble brown carbon (BrC) at Nanling background station in South China. *Front. Environ. Sci.* 12:1360453. doi: 10.3389/fenvs.2024.1360453

Seasonal changes in water-soluble brown carbon (BrC) at Nanling background station in South China

Bolong Zhang[1,2], Jiao Tang[1]*, Xiaofei Geng[1], Yangzhi Mo[1], Shizhen Zhao[1], Guangcai Zhong[1], Jun Li[1] and Gan Zhang[1]*

[1]State Key Laboratory of Organic Geochemistry and Guangdong Province Key Laboratory of Environmental Protection and Resources Utilization, Guangdong-Hong Kong-Macao Joint Laboratory for Environmental Pollution and Control, Guangzhou Institute of Geochemistry, Chinese Academy of Sciences, Guangzhou, China, [2]University of Chinese Academy of Sciences, Beijing, China

Brown carbon (BrC) is an important light-absorbing component of organic carbon (OC), causing large uncertainty in aerosol radiative forcing evaluation and being related to health issues as well. Knowledge of BrC in an atmospheric background station is beneficial to understand its role in a changing climate. A year-long sampling campaign was conducted at Nanling background station to get a comprehensive knowledge of WS-BrC, a total of seventy-two $PM_{2.5}$ samples throughout a year were used. Light absorption and fluorescence spectra of WSOC were analyzed synchronously using a fluorescence spectrophotometer. The low levels of $PM_{2.5}$, OC, and elemental carbon (EC) conferred a background site. The optical properties of WS-BrC were characterized using excitation-emission matrix (EEM) fluorescence spectroscopy. The WS-BrC made a significant contribution (365 nm, 18% $\pm$ 10%) to total carbonaceous aerosol absorption. The mass absorption efficiency (MAE) of WS-BrC is 0.81 $\pm$ 0.34 m^2 gC^{-1}, and varies among seasons due to the different sources or atmospheric processing. Three EEM fluorescent components were identified by parallel factor (PAFAFAC) analysis, including two humic-like substances (HULIS, C1, C2), and one phenolic-like component. The HULIS components accounted for approximately 70% of the total fluorescence intensities. Primary combustion emissions showed enhanced activity during the winter and spring seasons, but there were no significant influences on WS-BrC in spring. Secondary sources contributed significantly to WS-BrC during winter, summer, and autumn (all exceeding 50%), except for spring. Photooxidation is a significant process in the formation of secondary WS-BrC in winter and autumn, but there may be another formation pathway in summer, i.e., the ammonia pathway. This study contributes to our understanding of BrC in the background atmosphere.

KEYWORDS

brown carbon, fluorescence spectroscopy, source apportionment, photochemical process, atmospheric background station

1 Introduction

Carbonaceous aerosols have been a topic of concern due to their direct and indirect impact on climate change and human health (Shiraiwa et al., 2017; Liu et al., 2020). There are two main classes of carbonaceous aerosols: organic carbon (OC) and elemental carbon (EC, or black carbon [BC]) (Pöschl, 2003). EC is the main strong light-absorbing

component in the aerosols and exerts a warming effect, while OC was once considered as purely scatter solar radiation (Andreae and Gelencsér, 2006; Bond et al., 2011). However, in past decades, studies showed that certain types of OC efficiently absorb radiation in the near-ultraviolet (UV) and visible ranges, termed as brown carbon (BrC), which can positively contribute to the net direct radiation forcing (DRF) and offset the cooling effects of OC (Laskin et al., 2015; Wang et al., 2022). In addition, recent study has been observed that chromophores were also related to health issues, which are of greater public concern (Chen et al., 2019b).

Current estimates of the DRF of BrC with large uncertainty, ranging over more than one order of magnitude (0.04–0.57 W m^{-2}) (Feng et al., 2013; Lin et al., 2014; Wang et al., 2018; Zeng et al., 2020). The large uncertainty in current estimates of DRF is attributed to the large heterogeneity in the optical properties of BrC that vary depending on sources, aging processes, size distributions, and mixing states (Liu et al., 2015; Di Lorenzo et al., 2017; Chen et al., 2019a; Xu et al., 2019; Tang et al., 2020; Wang et al., 2022). Dasari et al. (2019) reported that the photochemical degradation of water-soluble BrC (WS-BrC) reduced light absorption during transport over 6,000 km in the Indo-Gangetic Plain (IGP). During over-ocean transit across the Bay of Bengal to an Indian Ocean receptor site, a first-order bleaching rate of 0.20 ± 0.05 day^{-1} was derived. Chen et al. (2019a) found that BrC chromophores with strong light absorption tend to be enriched in small particles. The high variability of BrC's optical properties indicates regional differences, with hotspots in South Asia IGP, Eastern Asia, the Amazon basin, the Indonesian region, and Southern Africa (Laskin et al., 2015). However, unlike BrC obtaining much more attention from urban, suburban, and remote areas such as the Tibetan plateau, limited studies have investigated BrC characteristics in regional atmospheric background sites, which are key to the assessment of anthropogenic impact on the environment at a regional scale.

China is a hotspot region with high loading of BrC (Wang et al., 2022; Xiong et al., 2022). The relevant research in regional background sites of China is crucial to evaluate the degree of regional radiative forcing resulting from BrC. Recently, Teich et al. (2017) studied the water-soluble and particulate BrC during summer in rural background sites (Xianghe, and Wangdu), located in the Hebei Province in the North China Plain (NCP). Li et al. (2023) investigated the fluorescence properties of BrC in fine particles in the background atmosphere of the NCP (at the Shangdianzi (SDZ) station). Zhao et al. (2021) reported a higher mass absorption efficiency (MAE) value of WS-BrC in a background Chongming Island in eastern China, located in the Yangtze River Delta (YRD) region, compared to that observed in an urban site (Mo et al., 2021). The Pearl River Delta (PRD) is one of the largest megacity clusters in the world, resulting from rapid economic growth and urbanization over the past few decades. Previous studies have investigated the light absorption of BrC in urban sites, including Guangzhou (Liu et al., 2018; Jiang et al., 2021; Mo et al., 2021; He et al., 2023), Hong Kong (Ma et al., 2019), and a semi-rural site, including Huaguoshan (Jiang et al., 2020). As far as we concerned, limited measurements of BrC have been conducted at regional atmospheric background stations in southern China, thus limiting the understanding of the impact of the city cluster. The Nanling background station locates in Nanling Mountain in South China, approximately 200 km far away from the PRD. Influenced by the East Asian monsoons, this area is the key pathway for the long-range transport of air pollutants between southern and central-eastern China (Gong et al., 2018; Lv et al., 2019), making it a suitable location to monitor the South China background regional BrC characteristic.

WS-BrC makes up a large fraction of BrC (Tang et al., 2021; Paraskevopoulou et al., 2023), here, we conducted a year-long campaign to sample aerosols to a comprehensive knowledge of WS-BrC aerosols at Nanling station. The objective was to recognize the chemical characteristics of carbonaceous aerosols and the optical properties, such as UV-vis absorption and fluorescence spectra, of WS-BrC at this background air station. Characteristics of WS-BrC sources were identified through the Potential Source Contribution Function (PSCF) model and molecular markers. We present a comprehensive study of WS-BrC at the atmospheric background station, which could help better constrain radiative forcing in the climate model.

2 Materials and methods

2.1 Sampling

Ambient samples of fine particulate matter ($PM_{2.5}$) were collected via a high-volume air sampler, operating at a rate of 1 m^3 min^{-1}, at this Nanling station (Figure 1, 112.898°E, 24.698°N, 1690 m a.s.l.) from 19 December 2017 to 22 December 2018. The sampling site is in Guangdong Province within a 273 km^2 national forest park. The area receives minimal emissions from anthropogenic activities, but is a significant recipient of air pollutant transport from northern China to the southern coastal region, especially during the winter monsoon period (Siu et al., 2005). The sampling period was divided into four seasons: winter (19 December 2017–28 February 2018), spring (March 9–15 May 2018), summer (June 11–22 August 2018), and autumn (September 18–29 November 2018). According to the 72-h air mass backward trajectories (Figure 1; Supplementary Figure S1), most air masses originated from the north continent and PRD, with only a small fraction originating from Southeast Asia and the ocean. In total, 72 $PM_{2.5}$ samples were collected during the sampling campaign. All samples were collected using pre-baked quartz fiber filters (QFFs, prebaked for 6 h at 450°C). After being collected, filter samples were immediately wrapped in baked aluminum foils and stored in a freezer (below −20°C) until analysis. The detailed sampling information during the sampling period are detailed in Supplementary Table S1 of the Supplementary Material.

2.2 Carbonaceous fraction, and optical properties measurements

The Sunset Laboratory OC/EC analyzer was used to determine the OC and EC, following the thermal/optical transmission method and the IMPROVE temperature protocol (Han et al., 2007). Water-soluble organic carbon (WSOC) was obtained by ultrasonication of QFFs samples with ultrapure water (resistivity >18.2 MΩ cm) for 30 min and filtering through a PTFE filter (0.22 μm, Anpel, China) to remove the undissolved particles and filter chips. The carbon

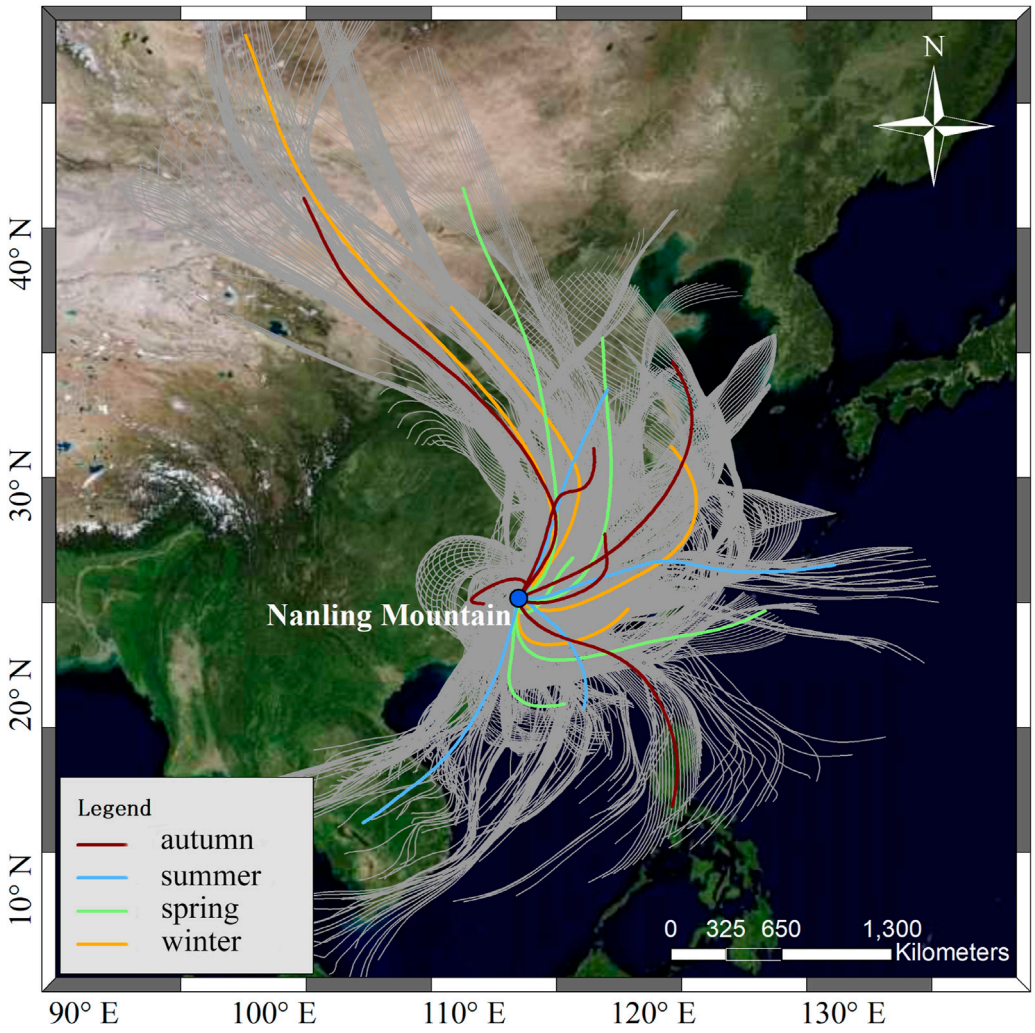

FIGURE 1
Atmospheric background sampling site at Nanling station. The 72-h backward trajectories at Nanling station for each season were analyzed by the HYSPLIT model, and more detail is shown in Supplementary Figure S1. The map was created using ArcGIS software, and the base map is from the National Platform for Common Geospatial Information Services (www.webmap.cn).

content of WSOC was measured using a total organic carbon analyzer (Vario TOC cube, Elementar, Germany), using non-purgeable organic carbon (NPOC) analysis mode. Prior to carbon content detection, phosphoric acid (Sigma-Aldrich) was added and purged with air to remove carbonates. A calibration curve for WSOC was created using a solution of potassium hydrogen phthalate ($C_8H_5KO_4$), and the correlation coefficient was above 0.999. Each sample was analyzed in triplicate, and the average value was reported.

Measurement of light absorption and fluorescence spectra of WSOC has already been presented (Tang et al., 2020; Tang et al., 2021). The light absorption and fluorescence spectra of the WSOC were analyzed synchronously using a fluorescence spectrophotometer (Aqualog, Horiba Scientific, USA). UV–Vis absorption spectra were scanned between 239 and 800 nm with 3 nm increments. The fluorescence spectra were recorded using an emission wavelength (Em) range of 247.01–825.03 nm and an excitation wavelength (Ex) range of 239–800 nm. The wavelength increments for Em and Ex were 4.66 and 3 nm, respectively. Before measurement, purified water was used for baseline correction.

All absorption data in this study were converted to an absorption coefficient at a given wavelength (Abs_λ, Mm^{-1}) using the equation provided by Hecobian et al. (2010) referring to Eq. (1):

$$Abs_\lambda = \frac{(A_\lambda - A_{700}) \times V_1 \times a \times \ln(10)}{Va \times a_1 \times l} \quad (1)$$

Here, A_λ is the value of light absorption at the given wavelength given by the spectrophotometer, and A_{700} refers to account for any drift; V_1 and a_1 is the volume of ultra-pure deionized water for extraction and the area of the extracted filter; Va is the volume of sampling air; l is the optical path length. The resulting absorption coefficient in units of m^{-1} was also converted from log base-10 to natural log to be consistent with how atmospheric measurements are typically reported.

The MAE and absorption Ångström exponent (AAE) are important optical parameters that reflect the light absorption

ability and spectral dependence of BrC, respectively (Cheng et al., 2011) referring to Eq. (2):

$$MAE_{\lambda} = \frac{Abs_{\lambda}}{C_i} \quad (2)$$

Here, C_i ($\mu g\, C/m^3$) is the concentration of WSOC after conversion to the atmosphere referring to Eq. (3).

$$\mathrm{MAE} = K \bullet \lambda^{-AAE} \quad (3)$$

Here, K is constant. In this study, the wavelength from 330 nm to 400 nm is selected for fitting the AAE value (Yan et al., 2015). The 300–400 nm range was chosen to 1) avoid interference from inorganic compounds at lower wavelengths, such as ammonium nitrate and nitrate ions (Bosch et al., 2014), and 2) ensure a sufficient signal-to-noise ratio for the samples studied. The $PM_{2.5}$ samples collected at the background station had low concentrations, especially during the summer, which could potentially introduce significant uncertainty when the wavelength exceeds 400 nm.

In addition, we estimated the relative light absorption contribution of WS-BrC to total aerosol light absorption by assuming that BrC and BC were externally mixed in aerosols (Cheng et al., 2011). Which is detailed in Tang et al. (2021) and Supplementary Text S1 in Supplementary Material.

The EEM datasets were decomposed using parallel factor (PARAFAC) analysis that referred to the study of Murphy et al. (2013), which was described in detail in our previous studies (Tang et al., 2020; Tang et al., 2021). Briefly, the EEM datasets were corrected for inner filter effects, and spectra normalization relative to the Raman peak area of ultrapure deionized water collected on the same day was performed to correct fluorescence in Raman Units (RU). The interpolation method was used to eliminate the signals of first-order Rayleigh, Raman, and second-order Rayleigh scattering from the EEM spectra. A PARAFAC model with two to seven components was explored, considering spectral loading, core consistency, and residual analysis (Supplementary Figures S2, S3). The three-PARAFAC solution passed the split-half validation (Supplementary Figure S4), indicating the model is stable.

2.3 Measurements of biomass-burning tracers

Levoglucosan was selected as the molecular marker for primary biomass burning (BB) emissions, which was analyzed using a derivatization method on a gas chromatograph-mass spectrometer (GC-MS) and was detailed in Geng et al. (2020). Internal standards (methyl-β-D-xylopyranoside) were added to the QFFs samples before 36-h Soxhlet extraction with DCM/methanol (93:7, v:v). Anhydrous sodium sulfate was used to remove any water. The polar organics were derivatized by adding 200 μL N,O-bis-trimethylsilyl-trifluoroacetamide (1% trimethylchlorosilane), and 100 μL anhydrous pyridine, and then heated at 70°C for 1 h. After sample derivatization, the residue was dried using nitrogen blowing, followed by the addition of 200 μL hexane before measurement on a GC-MS (Agilent GC7890 A coupled with 5975C MSD) equipped with a DB-5MS column (30 m × 0.25 mm × 0.25 μm). The recoveries of polar organics ranged from 69% to 113%.

2.4 Air mass back trajectories and potential source contribution function (PSCF) model

72-h back trajectories were generated by the Hybrid Single-particle Lagrangian Integrated Trajectory (HYSPLIT) model (http://www.arl.noaa.gov/HYSPLIT.php). Meteorological data were obtained from the Gridded Meteorological Data Archives of Air Resources Laboratory (ARL) (http://ready.arl.noaa.gov/archives.php). Trajectories were calculated at 1-h intervals and subjected to cluster analysis. The PSCF model can be applied for source region identification by dividing the potential source area into grid cells of $i \times j$, as detailed in our previous study (Geng et al., 2020). PSCF analysis yields $PSCF_{ij}$ values ranging from 0 to 1 in general, with higher $PSCF_{ij}$ indicating that the model has a higher probability of the ij_{th} cell being the source region. A limitation of PSCF-based approaches is the need to settle a weighing function to downweight cells associated with low residence time, which is usually observable as "trailing effects" (Petit et al., 2017). To investigate aerosol source partitioning and quantify the contribution of different aerosol emission sources and transport mechanisms, we performed weighted Potential Source Contribution Function (WPSCF) analysis. As PSCF represents a conditional probability, the error increases as the distance between the grid and sample points increases (Tiwari et al., 2018). In this study, the experimental area was divided into a 0.25° × 0.25° grid. The threshold value for calculating m_{ij} was set at the 75th percentile. To mitigate the impact of small n_{ij} values on PSCF, a weighting function was applied (Tiwari et al., 2018) referring to Eq. (4):

$$w_{ij} = \begin{cases} 1.00 & n_{ij} > 80 \\ 0.70 & 20 < n_{ij} \le 80 \\ 0.42 & 10 < n_{ij} \le 20 \\ 0.05 & n_{ij} \le 10 \end{cases} \quad (4)$$

3 Results and discussion

3.1 Abundances and seasonal variations of $PM_{2.5}$ and carbonaceous fractions

Table 1 summarizes the concentrations of chemical components, including OC, and EC, found in $PM_{2.5}$ at the Nanling background atmospheric station. $PM_{2.5}$ concentrations ranged from 1.3 to 43 $\mu g\, m^{-3}$ throughout the sampling period, with an average value of 13 ± 8.7 $\mu g\, m^{-3}$. The concentration levels followed a seasonal trend, with higher concentrations observed in spring (20 ± 11 $\mu g\, m^{-3}$), followed by winter (13 ± 8.1 $\mu g\, m^{-3}$), autumn (12 ± 7.2 $\mu g\, m^{-3}$), and summer (8.2 ± 5.0 $\mu g\, m^{-3}$). The concentration of $PM_{2.5}$ at the Nanling station is lower than that at the SDZ station (mean: about 27.5 $\mu g\, m^{-3}$), an atmospheric background station on the northern edge of the NCP (Li et al., 2023). The abundance of $PM_{2.5}$ collected at the Nanling station is much lower than that observed in urban sites in the PRD as summarized in the study of Tao et al. (2017). These findings imply

TABLE 1 Seasonal averages of organic carbon (OC), elemental carbon (EC), water-soluble organic carbon (WSOC), and biomass-burning tracer (levoglucosan) concentrations in $PM_{2.5}$ collected at the Nanling background station. Winter is from 19 December 2017, to 28 February 2018, spring is from March 9 to 15 May 2018, summer is from June 11 to 22 August 2018, and autumn is from September 18 to 29 November 2018.

	Annual (n = 72)	Winter (n = 18)	Spring (n = 14)	Summer (n = 21)	Autumn (n = 19)
$PM_{2.5}$ (μg m^{-3})	13 ± 8.7	13 ± 8.1	20 ± 11	8.2 ± 5.0	12 ± 7.2
Carbonaceous fractions (μg m^{-3})					
TC	2.4 ± 1.9	2.3 ± 1.5	5.3 ± 1.7	1.4 ± 0.65	1.4 ± 1.0
OC	1.6 ± 1.2	1.6 ± 1.1	3.0 ± 1.4	1.2 ± 0.59	1.2 ± 0.89
EC	0.75 ± 0.97	0.73 ± 0.50	2.2 ± 1.3	0.20 ± 0.08	0.27 ± 0.13
SOC	1.3 ± 1.0	1.3 ± 0.91	2.1 ± 1.6	1.1 ± 0.56	1.1 ± 0.85
POC	0.32 ± 0.41	0.31 ± 0.21	0.95 ± 0.53	0.09 ± 0.03	0.11 ± 0.05
char-EC	0.46 ± 0.78	0.49 ± 0.52	1.6 ± 1.0	0.01 ± 0.02	0.06 ± 0.09
soot-EC	0.30 ± 0.24	0.25 ± 0.08	0.63 ± 0.37	0.19 ± 0.07	0.21 ± 0.09
WSOC	0.95 ± 0.65	1.2 ± 0.87	0.99 ± 0.61	0.85 ± 0.56	0.81 ± 0.51
OC/EC	3.8 ± 2.3	2.3 ± 1.0	2.2 ± 2.7	5.8 ± 1.6	4.1 ± 1.7
SOC/OC	0.82 ± 0.17	0.78 ± 0.11	0.62 ± 0.24	0.93 ± 0.03	0.87 ± 0.07
WSOC/OC	0.66 ± 0.26	0.76 ± 0.21	0.37 ± 0.23	0.69 ± 0.24	0.75 ± 0.17
Char-EC/soot-EC	1.3 ± 2.3	2.4 ± 3.3	3.1 ± 2.1	0.06 ± 0.12	0.35 ± 0.60
[a]Levoglucosan	3.7 ± 8.5	7.4 ± 13	7.1 ± 10	0.61 ± 0.79	1.1 ± 1.5
Light absorption properties					
Abs_{365} (Mm^{-1})	0.89 ± 0.96	1.5 ± 1.5	0.68 ± 0.51	0.53 ± 0.39	0.86 ± 0.76
$Abs_{BrC,sec}(365)$ (Mm^{-1})	0.60 ± 0.82	1.1 ± 1.3	0.18 ± 0.39	0.41 ± 0.36	0.69 ± 0.71
$Abs_{BrC,sec}(365)/Abs_{365}$	0.55 ± 0.31	0.55 ± 0.26	0.13 ± 0.26	0.70 ± 0.17	0.70 ± 0.21
MAE_{365} (m^2/gC)	0.81 ± 0.34	1.0 ± 0.38	0.64 ± 0.30	0.61 ± 0.16	0.94 ± 0.29
AAE	5.3 ± 0.76	4.7 ± 0.66	5.4 ± 1.2	5.6 ± 0.42	5.4 ± 0.54
C1%	42% ± 7.7%	38% ± 8.6%	39% ± 10%	46% ± 4.9%	43% ± 3.5%
C2%	32% ± 9.5%	35% ± 7.8%	19% ± 8.5%	33% ± 6.9%	37% ± 6.1%
C3%	26% ± 15%	27% ± 16%	42% ± 17%	20% ± 8.5%	21% ± 8.9%

[a](ng m−3).

that Nanling station serves as an ideal regional atmospheric background station in southern China.

Total carbon (TC) is the sum of OC and EC and accounts for 23% ± 18% of $PM_{2.5}$ concentrations, indicating that carbonaceous aerosols are not major components of $PM_{2.5}$ in this atmospheric background station. Also, the proportion of total carbon in $PM_{2.5}$ is usually about 20.4~70% (Xu et al., 2015; 2020; Tan et al., 2016; Tao et al., 2017; Kaskaoutis et al., 2022), so the current results indicate that Nanling is less or rarely affected by combustion sources (Park and Yu, 2016; Kaskaoutis et al., 2024). In biomass burning experiments, TC can account for $PM_{2.5}$ with an average value of 51%–62% (Park and Yu, 2016). Kaskaoutis et al. (2022) reported very high contributions of TC to $PM_{2.5}$ in Ioannina (Greece) during winter, about more than 70%, which was affected by heavy biomass burning. As shown in Figure 2, OC concentrations ranged from 0.27 to 6.7 μg m^{-3} with an average value of 1.6 ± 1.2 μg m^{-3}. EC concentrations ranged from 0 to 5.3 μg m^{-3}, with an average value of 0.75 ± 0.97 μg m^{-3}. The OC concentrations in the Nanling mountain station were lower than those in the SDZ background station (OC: range: 0.66–23 μg m^{-3}, mean: 5.6 ± 4.0 μg m^{-3}) and Chongming Island (OC: 6.2 ± 3.3 μg m^{-3}), but EC had a comparable level to SDZ station (EC: range: 0–3.2 μg m^{-3}, mean: 0.70 ± 0.53 μg m^{-3}) (Zhao et al., 2021; Li et al., 2023). The average concentrations of OC and EC at the Nanling station were lower than those at other locations in the PRD, such as Guangzhou (OC: 7.55 ± 2.37 μg m^{-3} and EC: 2.86 ± 0.37 μg m^{-3} during autumn), Huaguoshan (8.09 ± 4.53 μg m^{-3} and 0.88 ± 0.38 μg m^{-3}), and Hong Kong (5 μg m^{-3} and 5.3 μg m^{-3}) (Jiang et al., 2020; Zhang et al., 2020; He et al., 2023). Thus, these values reflect the background characteristics of the study site, similar to Yaze village in the Tibetan Plateau (Zhang et al., 2021).

The ratio of OC to EC (OC/EC) ratio is usually used as the indicator of secondary organic carbon (SOC) and qualitative assessment of carbonaceous-aerosol sources, with values >2 previously indicating a contribution from SOA (Kunwar and Kawamura, 2014). Besides, high OC/EC ratio

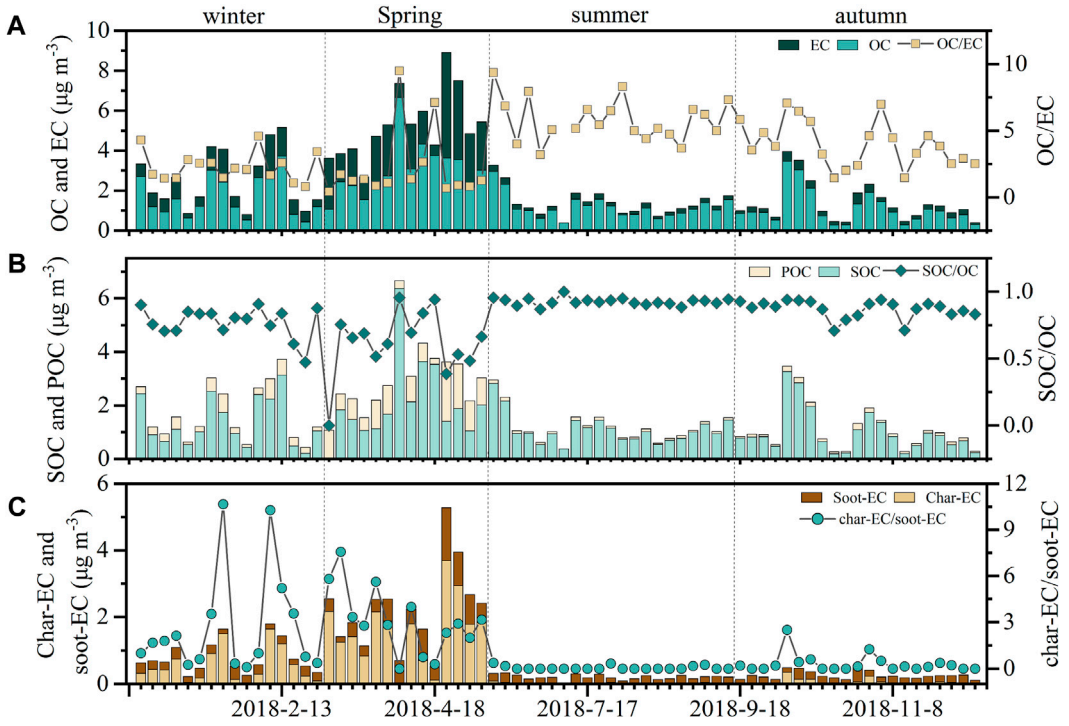

FIGURE 2
Time series plots of OC and EC and the ratio of OC to EC **(A)**, primary OC (POC) and secondary OC (SOC) and the ratio of SOC to OC **(B)**, and char-EC and soot-EC and the ratio of char-EC to soot-EC **(C)** in the $PM_{2.5}$ collected at Nanling background station during 2018.

values can indicate the presence of biomass burning aerosols (Park and Yu, 2016; Tang et al., 2020; Kaskaoutis et al., 2022). The OC/EC ratios varied from 0.42 to 9.5, with a mean value of 3.8 ± 2.3. The OC/EC ratios were higher in summer (5.8 ± 1.6) and autumn (4.1 ± 1.7) compared to winter (2.3 ± 1.0) and spring (2.2 ± 2.7) (Figure 2). Nearly 72% of the samples had OC/EC > 2, suggesting a potential source of SOA and biomass burning aerosols throughout the summer and autumn. However, the concentration of levoglucosan was significantly lower during the summer and autumn (refer to Table 1). This result suggests that particulate matter during summer and autumn was primarily associated with SOA sources. The remaining samples (OC/EC< 2) were mainly during the winter and spring, indicating that they may be influenced by a primary emission source, such as coal combustion or vehicle emissions (Grivas et al., 2012).

OC is primarily derived from primary OC (POC) and SOC. To investigate the contribution of SOC to OC, the EC-tracer method was used to separate the SOC and POC (Cao et al., 2004; Grivas et al., 2012; Shen et al., 2017) referring to Eq. (5) and Eq. (6):

$$POC = EC \times (OC/EC)_{pri} \quad (5)$$

$$SOC = OC_{tot} - POC \quad (6)$$

where OC_{tot} is the total of OC, and $(OC/EC)_{pri}$ is the OC/EC ratio considered representative of primary source emissions. This study used the minimum OC/EC ratio as the $(OC/EC)_{pri}$ during the study period, following previous studies (Cao et al., 2004; Li et al., 2015; Shen et al., 2017), to obtain an upper limit for SOC estimate (Pio et al., 2011; Grivas et al., 2012). The mean concentrations of SOC showed its highest level during spring (2.1 ± 1.6 μg m^{-3}), followed by winter (1.3 ± 0.91 μg m^{-3}), summer (1.1 ± 0.56 μg m^{-3}), and autumn (1.1 ± 0.85 μg m^{-3}), accounting for 62% ± 24%, 78% ± 11%, 93% ± 3%, and 87% ± 7% of OC, respectively (Figure 2). These results indicate that secondary sources have notably contributed to OC at the Nanling background station, while POC exhibited a relatively higher proportion during spring than in other seasons. This station appears to make a greater secondary contribution to OC compared to a previous study conducted in Xi'an (Shen et al., 2017), as well as Ioannina, Athens, and Heraklion (Kaskaoutis et al., 2020). However, it should be noted that the EC-tracer method could lead to an overestimation of POC due to the assumption that it is nonvolatile and nonreactive (Sudheer et al., 2016). Additionally, primary coal combustion and biomass burning have higher OC/EC ratios (Chen et al., 2005; Han et al., 2010), thus perhaps leading to an overestimate of SOC. Thus, it is important that the key of the EC tracer method is to find a proper primary OC/EC ratio (Srivastava et al., 2018). The main uncertainty in determining $(OC/EC)_{pri}$ is the lack of a definitive criterion for selecting a percentile that accurately represents $(OC/EC)_{pri}$, which can vary spatially and temporally (Wu et al., 2019; Kaskaoutis et al., 2020). The minimum R-squared (MRS) method is a more robust solution for estimate SOC compared to the $(OC/EC)_{min}$ and percentile methods (Wu and Yu, 2016). Kaskaoutis et al. (2020) reported that SOC estimates were previously obtained using the 5% and 25% percentiles of the OC/EC data to determine the $(OC/EC)_{pri}$, leading to results contrasting to the MRS approach in Ioannina (70%–74% for SOC). We also used the MRS method to determine the $(OC/EC)_{pri}$. A comparison of SOC estimates using the $(OC/EC)_{min}$ and MRS methods showed high correlations in this study (slopes = 1.008, R^2 = 0.94,

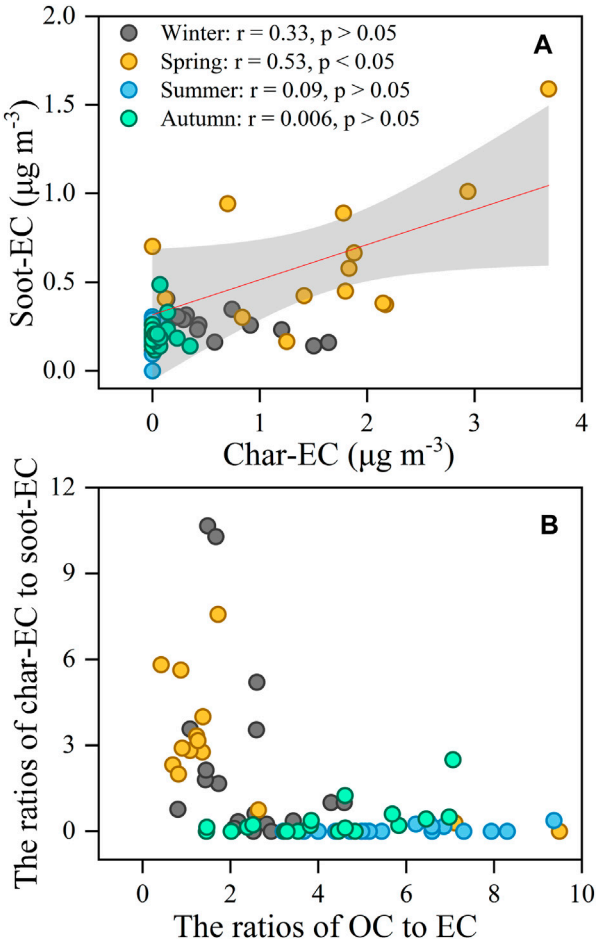

FIGURE 3
Correlations between char-EC and soot-EC in different seasons **(A)**, picture of the ratios of OC to EC and the ratios of char-EC to soot-EC from different seasons **(B)** at Nanling station. The red line represents the linear regression between char-EC and soot-EC during the spring, while the gray region shows 95% confidence bands.

Supplementary Figure S5). As reported in Kaskaoutis et al. (2020), the MRS method may significantly underestimate SOC levels in environments with high biomass burning. However, given that the low influence of biomass burning at Nanling mountain, this effect may be relatively small. This suggests that using the minimum OC/EC ratio to represent $(OC/EC)_{pri}$ for calculating SOC is reliable. The results implied the domination of SOC in the OC fraction of this station. The domination may be explained by the strong atmospheric oxidative capacity at this station (Gong et al., 2018).

The previous studies indicated that EC could be divided into char-EC and soot-EC according to their analytical method (Han et al., 2007; Han et al., 2010) referring to Eq. (7) and Eq. (8):

$$\text{char-EC} = \text{EC1} - \text{pyrolC} \quad (7)$$

$$\text{soot-EC} = \text{EC2} + \text{EC3} \quad (8)$$

Figure 2C shows the abundances of char-EC and soot-EC. At Nanling station, Char-EC, and soot-EC concentrations were very low, with average values of 0.46 ± 0.78 μg m^{-3} and 0.30 ± 0.24 μg m^{-3}in the annual year, respectively. The char-EC and soot-EC values are much lower than that reported in Xi'an (Char-EC: 6.86 ± 5.28 μg m^{-3}; soot-EC: 1.54 ± 0.64 μg m^{-3}) (Han et al., 2010) and Wusumu in a small village (Char-EC: 1.15 μg m^{-3}; soot-EC: 0.69 μg m^{-3}) (Han et al., 2008). The much higher char-EC portion was attributed to the relatively higher contributions of fuel (coal) consumption in Xi'an because coal combustion derived-EC is dominated by char-EC (Han et al., 2010). In the Nanling site, char-EC concentrations exhibited significant seasonal variability. The mean concentration value was 1.6 ± 1.0 μg m^{-3} in spring, 0.49 ± 0.52 μg m^{-3} in winter, 0.06 ± 0.09 μg m^{-3} in autumn, and 0.01 ± 0.02 μg m^{-3} in summer, accounting for 65% ± 26%, 49% ± 30%, 18% ± 20%, 5% ± 9.4%, respectively. The observed higher concentrations of char-EC in spring and winter may stem from local combustion emissions in the Nanling mountainous areas, such as biomass/coal combustion (Han et al., 2022). As mentioned above, the values of OC/EC were low in spring and summer, indicating that $PM_{2.5}$ in these two seasons had a coal combustion source. Atmospheric char particles possess larger sizes than soot, which facilitates the *in-situ* deposition of char and thus enables the reflection of local combustion emissions (Han et al., 2010). The soot-EC concentrations exhibit minor fluctuations throughout the year, with an increase in concentration during the spring. During this season, Figure 3A shows a clear correlation between char-EC and soot-EC, revealing a heightened presence of combustion sources that amplified the levels of both species. This indicates that during the spring, vehicle emissions also contribute to $PM_{2.5}$. However, soot-EC/EC ratios were found to increase from spring (35% ± 26%) and winter (51% ± 30%) to summer (98% ± 13%) and autumn (83% ± 22%). This suggests an increasing contribution of motor vehicle emissions. This could be assigned to be the background levels of soot that originate from vehicle emissions (Han et al., 2010). The char-EC/soot-EC ratio can serve as an indicator for source identification (Han et al., 2010). The mean char-EC/soot-EC ratio is 1.3 ± 2.3, with elevated values in spring (3.1 ± 2.1) and winter (2.4 ± 3.3), but consistently low values in summer (0.06 ± 0.12) and autumn (0.35 ± 0.60). The ratios of char-EC/soot-EC at Nanling station were much lower than the ratios in Xi'an (4.4 ± 3.27) (Han et al., 2010), Wusumu site (1.8) (Han et al., 2008), and Nanling (32–84) (Li et al., 2015). Generally, vehicle emissions exhibit low ratios of char-EC/soot-EC (<1) and OC/EC. Coal and biomass combustion, on the other hand, have higher ratios of char-EC/soot-EC (Han et al., 2022). Figure 3B shows that a significant majority of summer and autumn samples have low char-EC/soot-EC but higher OC/EC ratios, indicating vehicle emissions and additional secondary sources of aerosols during these seasons. However, the low concentrations of char-EC and soot-EC, and the high ratio of SOC/OC suggest that they may be associated with non-combustion SOA sources. All spring samples and a large portion of winter samples exhibit higher char-EC/soot-EC ratios, but low OC/EC ratios, indicating a local source of coal combustion emissions.

3.2 UV-vis light absorption properties of WS-BrC

The annual WSOC/OC ratio was 0.66 ± 0.26, higher in winter (0.76 ± 0.21), autumn (0.75 ± 0.17), and summer (0.69 ± 0.24) than

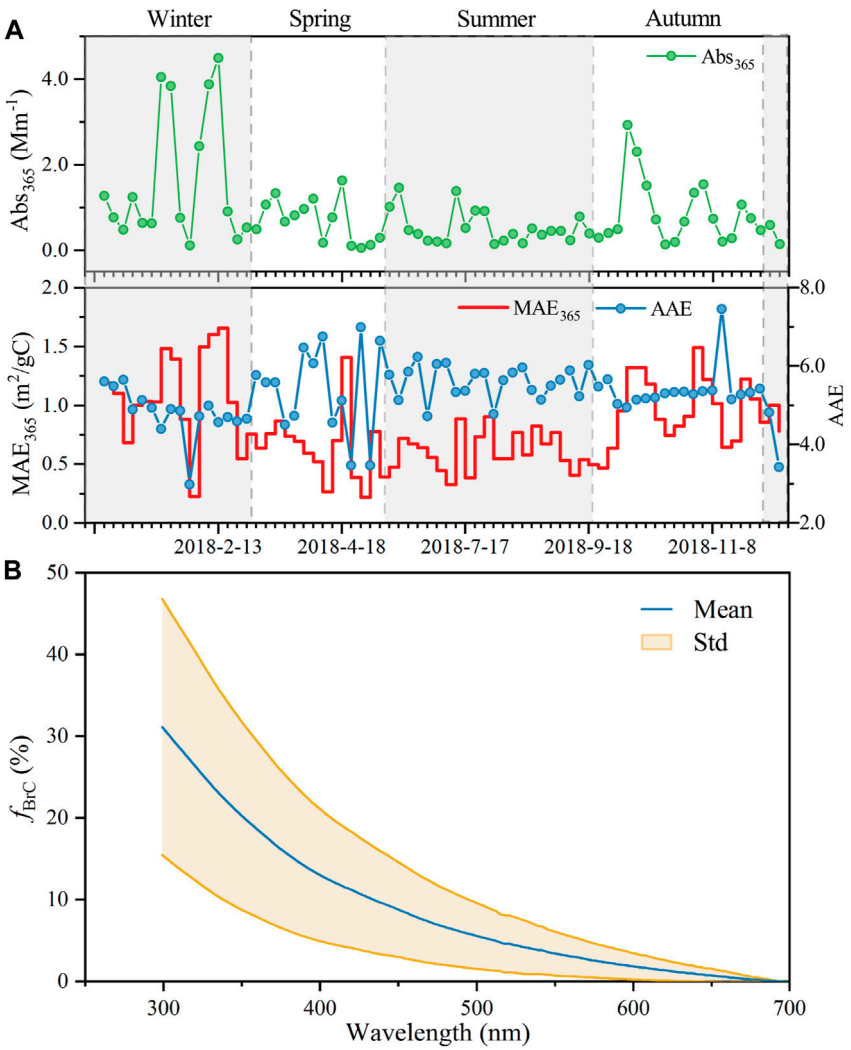

FIGURE 4
The seasonal and diurnal distributions of Abs_{365}, MAE_{365}, and AAE values **(A)**, and mean relative contribution of light absorption of WS-BrC to total aerosol absorption **(B)** in the $PM_{2.5}$ collected in atmospheric background station at Nanling Mountain.

in spring (0.37 ± 0.23). These ratios are well within the range of WSOC/OC ratios reported earlier (i.e., rural, marine and remote sites; Bosch et al., 2014; Lv et al., 2022; Wu et al., 2020; Yue et al., 2019). WS-BrC is an important light-absorption component in aerosols, as reported by Wu et al. (2019) and Tang et al. (2021). The Abs_{365}, which is commonly used as the proxy of BrC, ranged from 0.04 Mm^{-1} to 4.5 Mm^{-1} at Nanling station (Figure 4A), with an average of 0.89 ± 0.96 Mm^{-1}. The absorption coefficient at 365 nm at this station was comparable to that at Qomolangma Station (0.92 ± 0.97 Mm^{-1}) and higher than at Mt. Waliguan Baseline Observatory (0.30 ± 0.23 Mm^{-1}) in the Tibetan Plateau (Xu et al., 2020) and in high arctic atmospheric (0.07 ± 0.07 Mm^{-1}) (Yue et al., 2019), but much lower than that at the atmospheric background site in Chongming Island (5.39 ± 3.33 Mm^{-1}) (Zhao et al., 2021) and the urban site in Guangzhou (3.57 ± 1.34 Mm^{-1}) (Liu et al., 2018).

To better understand the significance of WS-BrC in this station, we estimated its relative light absorption contribution to total aerosol light absorption by assuming that BrC and BC are externally mixed in aerosols (Cheng et al., 2011), as described in Text S1. As shown in Figure 4B, WS-BrC plays a crucial role in the low-UV region (300 nm, 31%), but has a less contribution to longer wavelengths (e.g., 532 nm, 4.1%). Hoffer et al. (2006) estimated that HULIS, a significant component of WSOC, had a slight contribution to total light absorption at 532 nm and 35%–50% at 300 nm among Amazonia BB aerosols. Although light-absorbing OA may not be crucial for transferring total solar radiation in the troposphere when considering significant UV absorption at wavelengths below 300 nm, they can still cause a reduction in UV photolysis and near-surface ozone mixing ratios (Barnard et al., 2008). At Nanling station, WS-BrC accounted for an average of 18% of total aerosol light absorption at 365 nm, consistent with the observations in Godavari (Wu et al., 2019) and Bangkok (Tang et al., 2021). Srinivas et al. (2016) estimated that WS-BrC absorbs approximately 35% and 40% of solar radiation in day and night samples, respectively, relative to EC, from a source region of post-harvest agricultural waste burning in the IGP. In remote sites, smaller values were found for $PM_{2.5}$ collected on the central Tibetan Plateau and PM_{10} in the high Himalayas (Kirillova et al.,

2016; Zhang et al., 2020), where WS-BrC relative to BC were 13% ± 5% and 17% ± 8%, respectively. The variation in WS-BrC's contribution to total aerosol absorption in different regions is due to the effects of biomass burning and atmospheric aging due to water-soluble chromophores are more susceptible to photo-bleaching (Srinivas et al., 2016; Dasari et al., 2019; Paraskevopoulou et al., 2023). It is important to note that the measured absorption of BrC in water extracts may be underestimated by approximately two times compared to ambient conditions (Liu et al., 2013). A recent study found that the estimated ambient BrC absorption can be higher by a factor of 6, and severe residential wood burning can result in significant discrepancies (Paraskevopoulou et al., 2023). Furthermore, when the impact of biomass burning is moderate (levoglucosan <2 μg m^{-3}), the ratio of ambient BrC to WS-BrC is lower than 4 (Paraskevopoulou et al., 2023). In this study, the impact of biomass burning is very small (mean: 3.7 ± 8.5 ng m^{-3}), so the discrepancies caused by wood burning can be small. The difference in this study may be attributed to incomplete extraction of OC by solvents and size-dependent absorption properties of OA (Liu et al., 2013; Shetty et al., 2019). Therefore, the actual BrC impact could be more significant than the estimate provided in this study.

The MAE is a significant optical parameter that reflects the light absorption capability of BrC. Figure 4A illustrates that the MAE at 365 nm (MAE_{365}) varied between 0.22 and 1.7 m^2 gC^{-1}, with a mean value of 0.81 ± 0.34 m^2 gC^{-1}. The MAE_{365} exhibited a distinct seasonal pattern, with the peak value occurring during winter (1.0 ± 0.38 m^2 gC^{-1}), followed by autumn (0.94 ± 0.29 m^2 gC^{-1}) and spring (0.64 ± 0.30 m^2 gC^{-1}), and the lowest value in summer (0.61 ± 0.16 m^2 gC^{-1}). The seasonal difference in MAE values may be attributed to the different sources caused by monsoon and photochemical processing (Choudhary et al., 2021; Dasari et al., 2019). As mentioned above, $PM_{2.5}$ collected during winter and spring were more affected by primary coal combustion sources due to the increased char-EC/soot-EC, low OC/EC, and relatively low biomass burning tracer (e.g., levoglucosan). In contrast, $PM_{2.5}$ collected during summer and autumn were associated with non-combustion SOA sources. Coal combustion is a significant contributor to WS-BrC in the atmosphere (Yan et al., 2017; Tang et al., 2020). During long-distance transport, atmospheric photochemical oxidation also reduces the light absorption of BrC (Dasari et al., 2019). However, the value of WS-BrC in spring was lower than that in winter. The lower WSOC fractions in OC during spring could be attributed to enhanced emissions from coal combustion which produce a large fraction of water-insoluble organics (Yan et al., 2017; Li et al., 2018). The distinct MAE in summer and autumn is due to the different source regions of air masses. As shown in Supplementary Figure S1, during the autumn campaign, most air masses originated from the northern continent, but in summer, only a small fraction originated from the continent, while the majority came from the ocean. Continent-influenced air masses carried substances that absorb light stronger than marine-influenced air masses (Mo et al., 2022; Tang et al., 2024).

Compared to other remote sites, such as MCOH Northern region of Maldives (MCOH) (0.4 ± 0.11 and 0.46 ± 0.18 m^2 gC^{-1}) (Bosch et al., 2014; Dasari et al., 2019), Southeastern Tibetan Plateau (0.6 ± 0.19 m^2 gC^{-1}) (Zhang et al., 2021), and arctic (0.41 ± 0.39 m^2 gC^{-1}) (Yue et al., 2019), which are due to their locations at a high-altitude site or being influenced by the long-range transport, the average MAE_{365} at Nanling station is higher. However, the atmospheric WS-BrC at Nanling station has a light absorption capability comparable to that of Guangzhou (mean: 0.81 m^2 gC^{-1}) (He et al., 2023; Liu et al., 2018; Mo et al., 2021; Zhou et al., 2023), but lower than that of Huaguoshan (1.2 ± 0.24 m^2 gC^{-1}) (Jiang et al., 2020), and other urban sites like Beijing (Yan et al., 2015; Mo et al., 2018) and other Chinese cities in Mo et al. (2021). In the study by Ma et al. (2019), HULIS in Hong Kong had a MAE_{365} of 1.84 ± 0.77 m^2 gC^{-1}. Assuming that the MAE ratio of HULIS/WSOC is 1.4 according to Mo et al. (2018), the MAE of WSOC in Hong Kong is also higher than that of Nanling. Specifically, the MAE_{365} values were significantly lower compared to those obtained at IGP sites, such as Delhi and Kanpur (Dasari et al., 2019; Choudhary et al., 2021), as illustrated in Figure 5. Generally, atmospheric WS-BrC exhibits stronger light absorption capability in urban environments than in remote and rural regions less affected by anthropogenic activities. The differences in the absorption properties of WSOC at Nanling station, compared to those listed above, are attributed to their distinct source profiles (Laskin et al., 2015; Xiong et al., 2022). Nanling station is an atmospheric background station mainly derived from biogenic sources and relatively aged aerosols due to long-range transportation from urban regions. This may result in decrease the concentrations of aromatic chromophores in WSOC. Additionally, it is important to note that not all water-soluble organic compounds are light-absorbing. The light-absorbing properties of WSOC depend on the emission source, molecular structure, and aging processes (Dasari et al., 2019; Tang et al., 2020; Cao et al., 2021). Therefore, only certain parts of WSOC may contribute to light absorption (Yuan et al., 2020; Zhang et al., 2022). The calculated overall average ratios of BrC in OC (BrC/OC) in the anthropogenic and natural sources were about 29% ± 2% and 16% ± 2%, respectively (Xiong et al., 2022). Consequently, the reported MAE may be underestimated. Furthermore, WSOC masses were commonly utilized to determine the MAE of WS-BrC in previous studies (Hecobian et al., 2010; Cheng et al., 2011; Yan et al., 2015), making comparisons with other studies reliable.

AAE reflects both the wavelength dependence of light absorption and the degree of conjugation of the extracted compounds. The AAE values of WS-BrC that were fit between 330 and 400 nm were 5.3 ± 0.76 at this station (Figure 4A). The AAE values demonstrate a seasonal pattern that was lowest in winter (4.7 ± 0.66) and highest in summer (5.6 ± 0.42). The variability of AAE across different seasons indicate that BrC may be influenced by different sources or atmospheric processes (Dasari et al., 2019; Tian et al., 2019; Cao et al., 2021). The previous study indicated a steady increase in the WS-BrC AAE values resulting from the photolysis of chromophores and atmospheric oxidation during the long-range transport over the IGP (Dasari et al., 2019). In comparison to other studies (Figure 5B), AAE values at Nanling station are lower than those observed from MCOH (mean: about 7.0) (Bosch et al., 2014; Dasari et al., 2019), Korea Climate Observatory at Gosan (KCOG) (6.4 ± 0.6) (Kirillova et al., 2014), Southeastern Tibetan Plateau (7.08 ± 1.83) (Zhang et al., 2021), and comparable to those in Guangzhou in the PRD (He et al., 2023; Liu et al., 2018; Mo et al., 2021; Zhou et al., 2023), but higher than that observed from Huaguoshan (4.5 ± 0.62) (Jiang et al., 2020). Relatively low AAE at Nanling station indicates that the atmospheric WSOC has a weak wavelength dependence, suggesting different formation or emission sources compared to heavily populated regions. It is important to noted that

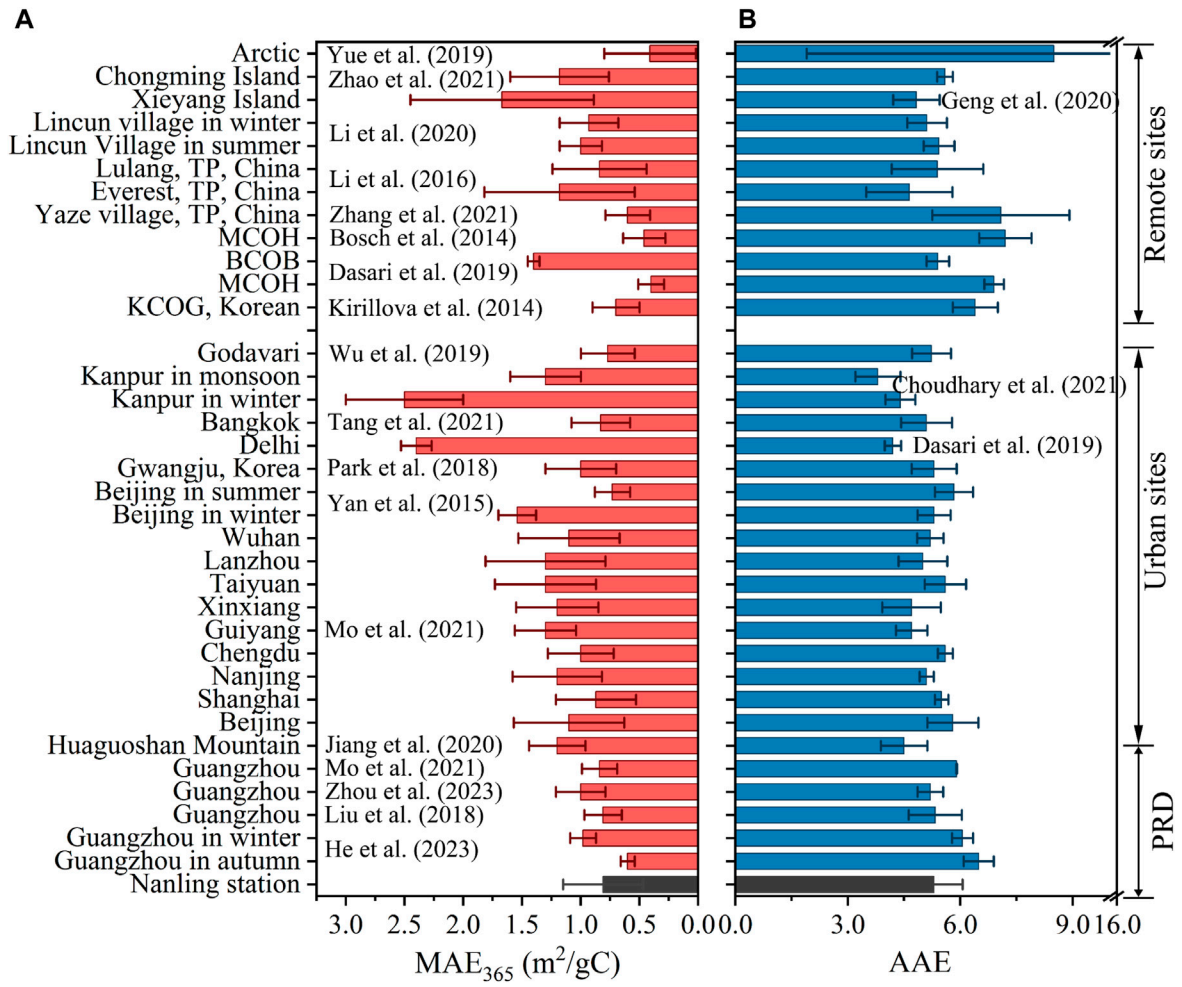

FIGURE 5
Comparison of light absorption of WS-BrC [**(A)** MAE_{365} (m^2/gC); **(B)** AAE] between Nanling station and other areas. The black columns represent our data. The detailed information is shown in Supplementary Table S2.

the wavelength band has a significant impact on AAE estimates. Therefore, most of the literature cited above has chosen the similar wavelength bands to make the comparisons more reliable. In a previous study, Mo et al. (2022) reported a good linear correlation between MAE_{365} and AAE, despite fitting AAE with different wavelength. This indicates that the aromatic component in WSOC is a crucial factor in determining its light absorption capacity. In addition, AAE values vary significantly across different locations worldwide and are influenced by various factors such as sources (Tian et al., 2019; Tang et al., 2020; Cao et al., 2021), atmospheric evolution (Dasari et al., 2019; Wong et al., 2019), OC polarity (Tang et al., 2021; Paraskevopoulou et al., 2023), and extraction methods (Zhang et al., 2013). Therefore, it is important to exercise caution when utilizing AAE values to determine BrC absorption.

3.3 Fluorescence components characteristics

Fluorescence spectra coupled with PARAFAC analysis can identify the chemical components of the BrC chromophores. This determination is crucial in understanding the characteristics of the absorbing components at the Nanling atmospheric background station. Figure 6A illustrates three fluorescent components that exhibited distinct patterns, suggesting their individual chemical information. C1 (ex/em = 305 nm/410 nm, 250 nm/410 nm) and C2 (ex/em = 355 nm/480 nm, 250 nm/480 nm) are classified as HULIS, while C3 (ex/em = 275/320 nm) is a phenolic-like component (Chen et al., 2016; Chen et al., 2020; Wu et al., 2021). A second peak in C1 and C2 was observed at a higher excitation wavelength, compared to C3, suggesting the presence of numerous condensed aromatic moieties, conjugated bonds, and nonlinear ring systems (Matos et al., 2015). These fluorescent components have been commonly detected in urban aerosol samples (Matos et al., 2015; He et al., 2023), the remote delta in the Tibetan Plateau (Wu et al., 2020; Zhang et al., 2021), and aging BB samples (Fan et al., 2020). In addition, similar fluorescent components observed in the Nanling background have also been identified at the SDZ atmospheric background station (Li et al., 2023). An additional component was detected at the SDZ station, perhaps indicating more complex pollution sources in SDZ than in the Nanling station.

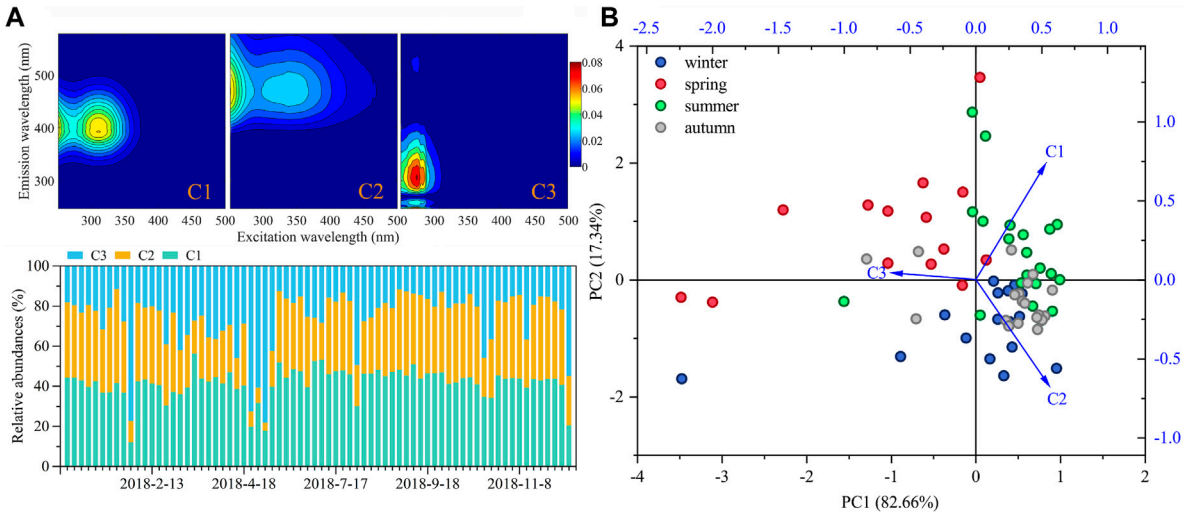

FIGURE 6
The fluorescent components identified (C1–3) by PARAFAC analysis and the times series of the relative contribution of C1–3 **(A)**, and principal components analysis (PCA) of C1–3 in the WSOC in $PM_{2.5}$ **(B)** collected in the Nanling background station during 2018.

The relative abundances of fluorescence intensities of C1–3 were used to indicate the variations in chemical compositions. Figure 6A shows that C1 is the most abundant chromophore and contributes 42% ± 7.7% to the total fluorescence intensity, followed by C2 (32% ± 9.5%). This indicates that HULIS components (C1 and C2) dominate the WS-BrC in $PM_{2.5}$ collected at this station, accounting for about 70% of the species. This fraction is lower than that in Godavari, where BB emissions are the dominant contribution of WS-BrC (about 80%) (Wu et al., 2019). C3 contributed the lowest contribution of total fluorescent intensities. In addition, the seasonal distribution of fluorescent chromophores exhibited varying patterns. The relative abundance of HULIS components (C1 and C2), is greater in summer (80% ± 8.5%) and autumn (79% ± 8.9%) than in winter (73% ± 16%) and spring (58% ± 17%). This suggests variations in sources and atmospheric processes across seasons. Previous studies have reported that these independent components possess distinct chemical properties, molecular compositions, and formation pathways (Chen et al., 2016; Jiang et al., 2022; Tang et al., 2024). Assuming the results show that the C1 and C2 components have a strong association with secondary sources, particularly C2, as observed in recent studies (Chen et al., 2021; Jiang et al., 2022; Li et al., 2023), C3 signifies a primary source. Li et al. (2023) found strong correlations at an atmospheric background station between the phenolic-like component and primary emission factors, such as fossil fuel combustion and biomass burning, as resolved by the positive matrix factorization (PMF) model. Deciphering the molecular composition of these fluorescent components reveals their availability. He et al. (2023) have found that the molecules associated with HULIS components have a higher oxidation degree ($\overline{OS}_C$) than the phenolic-like component, a quantity that is widely used to represent the oxidation degree of atmospheric OA (Kroll et al., 2011) and can reflect the secondary processes of compounds in the atmosphere. In our recent study, we utilized a similar method to identify the molecular components of HULIS and phenolic-like compounds (Tang et al., 2024). Our findings indicate that molecules linked to phenolic-like compounds are present in biomass burning organic aerosol (BBOA) and hydrocarbon-like organic aerosol (HOA) in the n_c-$\overline{OS}_C$ plot. Additionally, we discovered that oxidation reactions are the primary pathway for HULIS formation in the atmosphere. Thus, we further investigate the ratio of C3 to C1 and C2 (C3/(C1+C2)) to identify the sources in different seasons. The C3/(C1+C2) exhibits its highest level in spring (0.98), which is two to three times higher than those in winter (0.47), autumn (0.28), and summer (0.27) (Supplementary Figure S6). The humification index (HIX) indicates the degree of humification of WSOC. It is calculated by the ratio of the integrated fluorescence emission intensity in the region of 435–480 to 300–345 nm under the excitation wavelength of 254 nm (Tang et al., 2021). The HIX was found to increase significantly with aging (Lee et al., 2013; Fan et al., 2020). Li et al. (2023) demonstrated that HIX correlates well with secondary formation factors. Jung et al. (2023) found a strong correlation between humic-like/protein-like ratios and HIX. In contrast, we observed a significant negative correlation between C3/(C1+C2) and HIX (Spearman's coefficient = −0.92, $p < 0.01$), indicating that the C3/(C1+C2) ratio is a useful indicator of primary sources of chromophores. These results suggest that primary sources had a greater impact on chromophores during the spring.

To further characterize the potential source of chromophoric WSOC in four seasons, we utilized a principal component analysis (PCA) of relative fluorescence intensities, a method similar to Chen H. et al. (2017). The fluorescence intensity percentages of the fitted PARAFAC components can effectively identify the chromophore types of WS-BrC in different seasons. According to the arrows (C1, C2, and C3) on the *x*-axis and *y*-axis, it appears that variables of C3 primarily contributed to PC1 according to its square cosines, but were negatively correlated. Variables C1 and C2 had a high loading on PC2, but variable C2 was negatively correlated. The scores for each season formed a distinct cluster. As shown in Figure 6B, samples in winter and autumn contained only the C2 component. The analysis revealed a positive correlation between these samples and PC1, but a negative correlation with PC2. The samples collected in spring were found to have a distinct

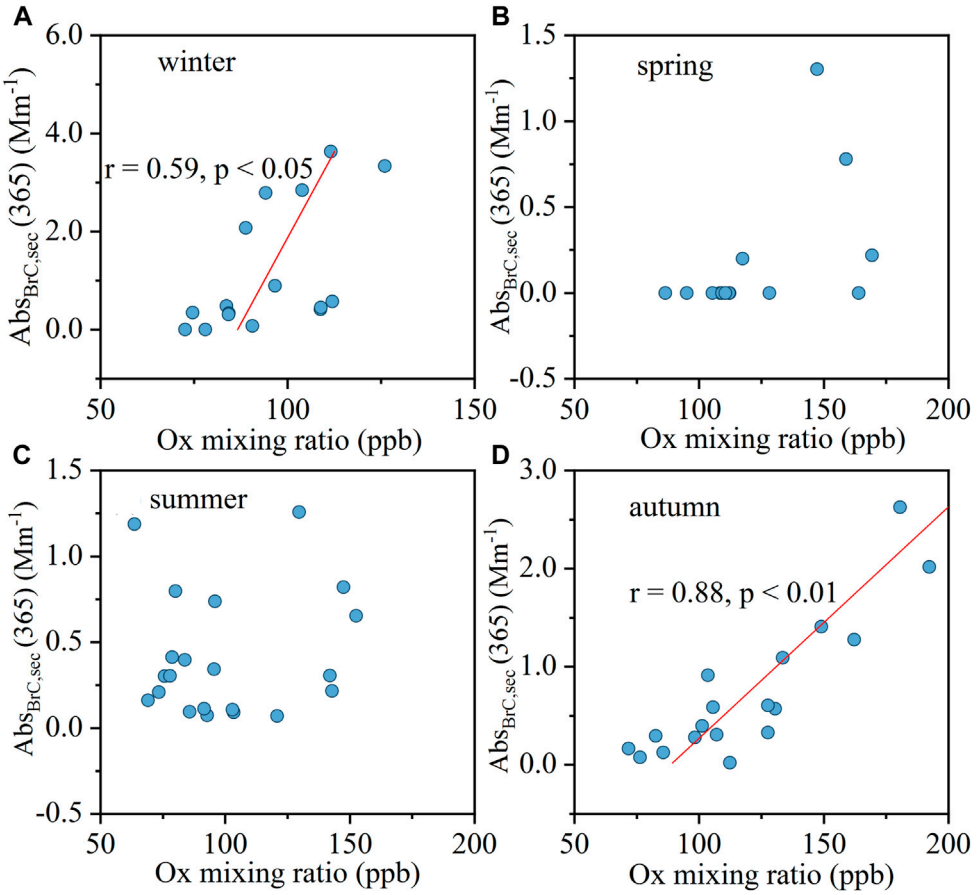

FIGURE 7
The relationship between secondary WS-BrC (Abs$_{BrC,sec}$ (365)) and O_x (O_x = NO_2 +O_3) in the four seasons **(A–D)**.

source and status compared to those collected in winter and autumn, which justifies their unique characteristic as discussed above. In contrast, most of the samples collected in summer showed a positive correlation with both PC1 and PC2. As discussed above, samples in winter and autumn were mainly driven by C2 component. In our recent research, Tang et al. (2021) observed that the PARAFAC component with the longest emission maxima had the largest coefficient in fitting light absorption and PARAFAC components through multiple linear regression. Niu et al. (2022) reported that a PARAFAC component in snow samples, similar to our C2, substantially contributes to the light absorption of WSOC at UV wavelengths. This could potentially account for the higher MAE values of WS-BrC during winter and autumn rather than spring and summer.

3.4 Potential origins and atmospheric processes of WS-BrC at Nanling background station

As presented above, the carbonaceous components (OC, EC) and optical properties of WS-BrC in $PM_{2.5}$ collected at Nanling atmospheric background station varied significantly in different seasons. Therefore, it is essential to identify the sources contributing to the different optical characteristics. EC is primarily produced through the incomplete combustion of biomass and fossil fuels (Bond et al., 2004). It consists of char-EC and soot-EC. Abs_{365} showed a strong positive correlation with char-EC in winter, summer, and autumn (Supplementary Table S3), despite the fact that the level of char-EC in summer and autumn is significantly lower than that in winter. During the spring season, the concentration of EC was at its highest, with low OC/EC, and high char-EC and soot-EC concentrations. This suggests that BrC in spring may be more affected by primary combustion emissions, such as fossil-fuel combustions (coal combustion and vehicles). Additionally, the primary combustion-derived BrC may be less water-soluble, resulting in low WSOC/OC during spring. A previous study indicated that the lower WSOC fractions in OC during winter were attributed to increased emissions from coal combustion, which produce a significant portion of water-soluble organics (Yan et al., 2017). Furthermore, only Abs_{365} was positively associated with soot-EC during summer. Soot-EC in this season could be attributed to be the background levels of soot that originate from vehicle emissions, as mentioned above. Thus, it may have a minor impact on WS-BrC during this season.

Levoglucosan is a commonly used tracer of BB emissions because it is a monosaccharide derivative produced only from the breakdown of cellulose during BB emissions (Simoneit, 2002). The

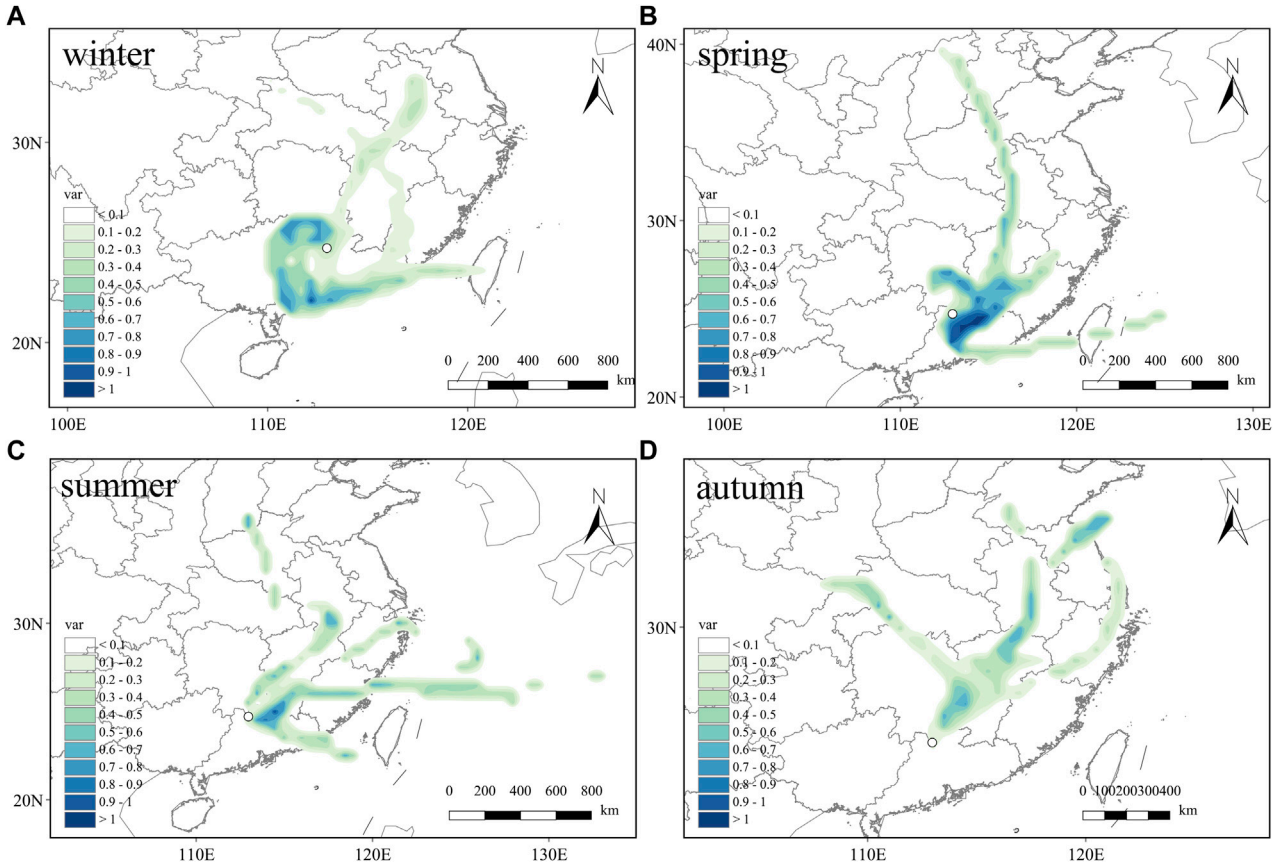

FIGURE 8
PSCF analysis of water-soluble BrC [Abs_{365}, **(A–D)**] in $PM_{2.5}$ samples collected in atmospheric background station at Nanling mountain in different seasons.

average concentration of levoglucosan in winter (7.4 ng m^{-3}) is comparable to that in spring (7.1 ng m^{-3}). However, it is 7–10 times higher than the concentrations in autumn (1.1 ng m^{-3}) and summer (0.61 ng m^{-3}) (Table 1). This suggests enhanced biomass-burning influence in the winter and spring, as indicated by the higher number of fire dots in those seasons (Supplementary Figure S1). The correlation between Abs_{365} and levoglucosan were positive during the winter and spring, which suggests that biomass burning potentially influences the WS-BrC. However, it is important to note that the concentration of levoglucosan at the Nanling station is significantly lower than in other regions, for instance, in Godavari (Nepal) (56 ± 66 ng m^{-3}, Wu et al., 2019), Bangkok (Thailand) (170 ± 205 ng m^{-3}, Wang et al., 2020), Guangzhou (115 ± 90 ng m^{-3}, Kuang et al., 2015), Huaguoshan (145 ± 87 ng m^{-3}, Jiang et al., 2020), Xieyang Island (21 ± 36 ng m^{-3}, Geng et al., 2019), and Chongming Island (Zhao et al., 2021). The concentration at the Nanling station was found to be similar to that in the Arctic Ocean (0.37 ng m^{-3}, Fu et al., 2013), indicating a low level of biomass-burning activity and representing the background level at this station. This suggests a limited influence of BB on WS-BrC at the Nanling background station.

The discussions above demonstrated that SOC significantly contributed to OC in $PM_{2.5}$ at Nanling station, indicating a predominant secondary source. Abs_{365} showed a strong correlation with SOC concentrations (Supplementary Table S3), except for spring, implying a secondary source of WS-BrC in these seasons. To investigate the secondary source of WS-BrC, we used the minimum R-squared (MRS) method to separate light absorption by secondary and primary BrC (Wu and Yu, 2016; Wang et al., 2019), as described in Text S2. On average, the secondary WS-BrC at 365 nm ($Abs_{BrC,sec}$ (365)) accounted for 55% of WS-BrC, with the highest contributions in autumn and summer (both 70%), followed by winter (55%). This suggests a significant secondary source of WS-BrC in winter, summer, and autumn (Table 1). However, the secondary WS-BrC only contributed 13% in spring, which is consistent with the primary fossil-fuel emissions presented above for this season. A previous study has demonstrated that odd oxygen ($Ox = NO_2 + O_3$) can serve as an indicator of air mass aging resulting from photochemical reactions (Wang et al., 2019). Strong positive correlations between $Abs_{BrC,sec}$ (365) and Ox were observed during winter and autumn (r = 0.59, and 0.88, respectively), indicating that photolysis or photooxidation caused secondary BrC chromophores (Figure 7). However, the absence of correlation in summer may suggest other secondary reactions contributing to the formation of WS-BrC during this season. During the summer, a positive correlation was observed between $Abs_{BrC,sec}$ (365) and NH_4^+ (Supplementary Figure S7). Liu et al.

(2023) reported that ammonia had an enhancing effect on BrC formation in China, particularly during humid haze periods.

Figure 8 illustrates the PSCF model, highlighting different geographical locations relative to WS-BrC at the Nanling background station. The analysis of the weighted potential source contribution function (WPSCF) for Abs_{365} is conducted on a seasonal basis. The potential source areas of WS-BrC in winter and spring are linked to adjacent regions. During winter, the potential source areas of WS-BrC are mainly in Guangdong and Guangxi Provinces, along with PRD. In the PRD, industrial emissions, including the ceramic industry and coal combustion, were the most important sources, followed by vehicles, which accounted for 39.2% and 20%, respectively (Tan et al., 2016). This consists well with above discussion that the high contribution from fossil fuel combustion (mainly coal combustion) is in winter. However, during spring, WS-BrC has the highest potential source areas from local emissions, including the Northern Guangdong (NE-GD) Provinces. Air masses mostly come from the adjacent Shaoguan City, thus being influenced by vehicles, which results in increased soot-EC concentration. Additionally, industry sources are the major contributors, accounting for 21.5%–23.6% of those in the NE-GD region (Xin et al., 2017). During the summer, the aerosol samples were affected by monsoons. WS-BrC may originate from two potential source areas: the northern regions, such as Jiangxi and Fujian Provinces, and the marine area, which carries fewer chromophores in the air masses. In autumn, air masses from Jiangsu, Jiangxi, and Anhui Provinces can travel long distances to reach the Nanling station. Crop residue burning occurs mainly in October-November, with corn residue burning being prevalent in North China and second season rice straw burning in South China (Chen et al., 2017; Ke et al., 2019). The burning of crop residue releases abundant air masses with strong chromophores, which enhances the light absorption capacity of WS-BrC. The low concentration of levoglucosan during this season is due to its short atmospheric lifetime (Wong et al., 2019). These findings indicate that the source regions of WS-BrC were strongly linked to chemical aerosol properties described above and their source fingerprints.

4 Conclusion

In this study, the light absorption of WS-BrC in $PM_{2.5}$ at Nanling background station in South China was investigated. The main conclusions were showed as follows:

(1) The $PM_{2.5}$, OC, and EC exhibited a low concentration compared to the adjacent region or other background sites, indicating a background level over South China. The station was influenced by strong secondary processes (high SOC/OC), while the samples collected during winter and spring were influenced by possible local combustion emissions (higher char-EC concentrations and char-EC/soot-EC ratios, but low OC/EC), i.e., fossil-fuel combustion.

(2) As a proxy for BrC, WS-BrC also contributes a significant portion of total aerosol absorption, particularly in the near-UV region. The MAE_{365} of WS-BrC at this station is variable across different seasons, mainly attributing to the different sources and atmospheric processing. Even though lower levels of carbonaceous aerosols were observed at Nanling station than those in the PRD, the MAE_{365} of WS-BrC was comparable to those in Guangzhou but lower than that observed in Huaguoshan and Hong Kong in the PRD, suggesting an ideal atmospheric background station to assess the anthropogenic impacts from the PRD region on the atmospheric radiative forcing in South China.

(3) This study also investigated the potential sources of WS-BrC by correlating them with molecular tracers and separating the primary and secondary WS-BrC using an MRS method. Higher activity of primary combustion emissions during spring and winter, compared to other seasons, may not significantly influence WS-BrC in spring due to its low light absorption. Secondary WS-BrC contributes significantly to WS-BrC during winter, summer, and autumn, but only minimally during spring. Photooxidation is a significant process in the formation of secondary WS-BrC in winter and autumn. However, in summer, there may be another formation pathway, i.e., the ammonia pathway.

This study provides detailed information on the light absorption and sources of WS-BrC in the background atmosphere. The findings will improve our understanding of BrC at the atmospheric background station and will serve as a reference for background levels to assess BrC's radiative effect in South China.

Data availability statement

The original contributions presented in the study are included in the article/Supplementary Material, further inquiries can be directed to the corresponding authors.

Author contributions

BZ: Data curation, Formal Analysis, Investigation, Writing–original draft. JT: Conceptualization, Data curation, Methodology, Writing–review and editing. XG: Methodology, Writing–review and editing. YM: Methodology, Writing–review and editing. SZ: Funding acquisition, Resources, Writing–review and editing. GuZ: Resources, Writing–review and editing. JL: Resources, Supervision, Writing–review and editing. GaZ: Conceptualization, Funding acquisition, Methodology, Project administration, Resources, Supervision, Writing–review and editing.

Funding

The author(s) declare financial support was received for the research, authorship, and/or publication of this article. This research has been supported by the National Natural Science Foundation of China (Grant Nos 42030715 and 42192511), the Alliance of International Science Organizations (ANSO-CR-KP-2021-05), the Guangdong Basic and Applied Basic Research Foundation (2021A0505020017 and 2023B1515020067), the Youth Innovation Promotion Association, CAS (2022359).

Conflict of interest

The authors declare that the research was conducted in the absence of any commercial or financial relationships that could be construed as a potential conflict of interest.

Publisher's note

All claims expressed in this article are solely those of the authors and do not necessarily represent those of their affiliated organizations, or those of the publisher, the editors and the reviewers. Any product that may be evaluated in this article, or claim that may be made by its manufacturer, is not guaranteed or endorsed by the publisher.

Supplementary material

The Supplementary Material for this article can be found online at: https://www.frontiersin.org/articles/10.3389/fenvs.2024.1360453/full#supplementary-material

References

Andreae, M. O., and Gelencsér, A. (2006). Black carbon or brown carbon? The nature of light-absorbing carbonaceous aerosols. *Atmos. Chem. Phys.* 6, 3131–3148. doi:10.5194/acp-6-3131-2006

Barnard, J. C., Volkamer, R., and Kassianov, E. I. (2008). Estimation of the mass absorption cross section of the organic carbon component of aerosols in the Mexico City Metropolitan Area. *Atmos. Chem. Phys.* 8, 6665–6679. doi:10.5194/acp-8-6665-2008

Bond, T. C., Streets, D. G., Yarber, K. F., Nelson, S. M., Woo, J.-H., and Klimont, Z. (2004). A technology-based global inventory of black and organic carbon emissions from combustion. *J. Geophys. Res.-Atmos.* 109. doi:10.1029/2003jd003697

Bond, T. C., Zarzycki, C., Flanner, M. G., and Koch, D. M. (2011). Quantifying immediate radiative forcing by black carbon and organic matter with the Specific Forcing Pulse. *Atmos. Chem. Phys.* 11, 1505–1525. doi:10.5194/acp-11-1505-2011

Bosch, C., Andersson, A., Kirillova, E. N., Budhavant, K., Tiwari, S., Praveen, P. S., et al. (2014). Source-diagnostic dual-isotope composition and optical properties of water-soluble organic carbon and elemental carbon in the South Asian outflow intercepted over the Indian Ocean. *J. Geophys. Res.-Atmos.* 119 (11), 11,743–11,759. doi:10.1002/2014jd022127

Cao, J. J., Lee, S. C., Ho, K. F., Zou, S. C., Fung, K., Li, Y., et al. (2004). Spatial and seasonal variations of atmospheric organic carbon and elemental carbon in Pearl River Delta Region, China. *Atmos. Environ.* 38, 4447–4456. doi:10.1016/j.atmosenv.2004.05.016

Cao, T., Li, M., Zou, C., Fan, X., Song, J., Jia, W., et al. (2021). Chemical composition, optical properties, and oxidative potential of water- and methanol-soluble organic compounds emitted from the combustion of biomass materials and coal. *Atmos. Chem. Phys.* 21, 13187–13205. doi:10.5194/acp-21-13187-2021

Chen, H., Liao, Z. L., Gu, X. Y., Xie, J. Q., Li, H. Z., and Zhang, J. (2017a). Anthropogenic influences of paved runoff and sanitary sewage on the dissolved organic matter quality of wet weather overflows: an excitation-emission matrix parallel factor analysis assessment. *Environ. Sci. Technol.* 51, 1157–1167. doi:10.1021/acs.est.6b03727

Chen, J., Li, C., Ristovski, Z., Milic, A., Gu, Y., Islam, M. S., et al. (2017). A review of biomass burning: emissions and impacts on air quality, health and climate in China. *Sci. Total Environ.* 579, 1000–1034. doi:10.1016/j.scitotenv.2016.11.025

Chen, Q., Hua, X., Li, J., Chang, T., and Wang, Y. (2021). Diurnal evolutions and sources of water-soluble chromophoric aerosols over Xi'an during haze event, in Northwest China. *Sci. Total Environ.* 786, 147412. doi:10.1016/j.scitotenv.2021.147412

Chen, Q., Li, J., Hua, X., Jiang, X., Mu, Z., Wang, M., et al. (2020). Identification of species and sources of atmospheric chromophores by fluorescence excitation-emission matrix with parallel factor analysis. *Sci. Total Environ.* 718, 137322. doi:10.1016/j.scitotenv.2020.137322

Chen, Q., Miyazaki, Y., Kawamura, K., Matsumoto, K., Coburn, S., Volkamer, R., et al. (2016). Characterization of chromophoric water-soluble organic matter in urban, forest, and marine aerosols by HR-ToF-AMS analysis and excitation-emission matrix spectroscopy. *Environ. Sci. Technol.* 50, 10351–10360. doi:10.1021/acs.est.6b01643

Chen, Q., Mu, Z., Song, W., Wang, Y., Yang, Z., Zhang, L., et al. (2019a). Size-resolved characterization of the chromophores in atmospheric particulate matter from a typical coal-burning city in China. *J. Geophys. Res.-Atmos.* 124, 10546–10563. doi:10.1029/2019jd031149

Chen, Q., Wang, M., Wang, Y., Zhang, L., Li, Y., and Han, Y. (2019b). Oxidative potential of water-soluble matter associated with chromophoric substances in $PM_{2.5}$ over xi'an, China. *Environ. Sci. Technol.* 53, 8574–8584. doi:10.1021/acs.est.9b01976

Chen, Y. J., Sheng, G. Y., Bi, X. H., Feng, Y. L., Mai, B. X., and Fu, J. M. (2005). Emission factors for carbonaceous particles and polycyclic aromatic hydrocarbons from residential coal combustion in China. *Environ. Sci. Technol.* 39, 1861–1867. doi:10.1021/es0493650

Cheng, Y., He, K. B., Zheng, M., Duan, F. K., Du, Z. Y., Ma, Y. L., et al. (2011). Mass absorption efficiency of elemental carbon and water-soluble organic carbon in Beijing, China. *Atmos. Chem. Phys.* 11, 11497–11510. doi:10.5194/acp-11-11497-2011

Dasari, S., Andersson, A., Bikkina, S., Holmstrand, H., Budhavant, K., Satheesh, S., et al. (2019). Photochemical degradation affects the light absorption of water-soluble brown carbon in the South Asian outflow. *Sci. Adv.* 5, eaau8066. doi:10.1126/sciadv.aau8066

Di Lorenzo, R. A., Washenfelder, R. A., Attwood, A. R., Guo, H., Xu, L., Ng, N. L., et al. (2017). Molecular-size-Separated Brown carbon absorption for biomass-burning aerosol at multiple field sites. *Environ. Sci. Technol.* 51, 3128–3137. doi:10.1021/acs.est.6b06160

Fan, X. J., Cao, T., Yu, X. F., Wang, Y., Xiao, X., Li, F. Y., et al. (2020). The evolutionary behavior of chromophoric brown carbon during ozone aging of fine particles from biomass burning. *Atmos. Chem. Phys.* 20, 4593–4605. doi:10.5194/acp-20-4593-2020

Feng, Y., Ramanathan, V., and Kotamarthi, V. R. (2013). Brown carbon: a significant atmospheric absorber of solar radiation? *Atmos. Chem. Phys.* 13, 8607–8621. doi:10.5194/acp-13-8607-2013

Fu, P. Q., Kawamura, K., Chen, J., Charrière, B., and Sempéré, R. (2013). Organic molecular composition of marine aerosols over the Arctic Ocean in summer: contributions of primary emission and secondary aerosol formation. *Biogeosciences* 10, 653–667. doi:10.5194/bg-10-653-2013

Geng, X., Mo, Y., Li, J., Zhong, G., Tang, J., Jiang, H., et al. (2020). Source apportionment of water-soluble brown carbon in aerosols over the northern South China Sea: influence from land outflow, SOA formation and marine emission. *Atmos. Environ.* 229, 117484. doi:10.1016/j.atmosenv.2020.117484

Geng, X., Zhong, G., Li, J., Cheng, Z., Mo, Y., Mao, S., et al. (2019). Molecular marker study of aerosols in the northern South China sea: impact of atmospheric outflow from the Indo-China peninsula and South China. *Atmos. Environ.* 206, 225–236. doi:10.1016/j.atmosenv.2019.02.033

Gong, D., Wang, H., Zhang, S., Wang, Y., Liu, S. C., Guo, H., et al. (2018). Low-level summertime isoprene observed at a forested mountaintop site in southern China: implications for strong regional atmospheric oxidative capacity. *Atmos. Chem. Phys.* 18, 14417–14432. doi:10.5194/acp-18-14417-2018

Grivas, G., Cheristanidis, S., and Chaloulakou, A. (2012). Elemental and organic carbon in the urban environment of Athens. Seasonal and diurnal variations and estimates of secondary organic carbon. *Sci. Total Environ.* 414, 535–545. doi:10.1016/j.scitotenv.2011.10.058

Han, Y., Chen, Y., Feng, Y., Shang, Y., Li, J., Li, Q., et al. (2022). Existence and formation pathways of high- and low-maturity elemental carbon from solid fuel combustion by a time-resolved study. *Environ. Sci. Technol.* 56, 2551–2561. doi:10.1021/acs.est.1c05216

Han, Y. M., Cao, J. J., Chow, J. C., Watson, J. G., An, Z. S., Jin, Z. D., et al. (2007). Evaluation of the thermal/optical reflectance method for discrimination between char- and soot-EC. *Chemosphere* 69, 569–574. doi:10.1016/j.chemosphere.2007.03.024

Han, Y. M., Cao, J. J., Lee, S. C., Ho, K. F., and An, Z. S. (2010). Different characteristics of char and soot in the atmosphere and their ratio as an indicator for source identification in Xi'an, China. *Atmos. Chem. Phys.* 10, 595–607. doi:10.5194/acp-10-595-2010

Han, Y. M., Han, Z. W., Cao, J. J., Chow, J. C., Watson, J. G., An, Z. S., et al. (2008). Distribution and origin of carbonaceous aerosol over a rural high-mountain lake area, Northern China and its transport significance. *Atmos. Environ.* 42, 2405–2414. doi:10.1016/j.atmosenv.2007.12.020

He, T., Wu, Y., Wang, D., Cai, J., Song, J., Yu, Z., et al. (2023). Molecular compositions and optical properties of water-soluble brown carbon during the autumn and winter in Guangzhou, China. *Atmos. Environ.* 296, 119573. doi:10.1016/j.atmosenv.2022.119573

Hecobian, A., Zhang, X., Zheng, M., Frank, N., Edgerton, E. S., and Weber, R. J. (2010). Water-Soluble Organic Aerosol material and the light-absorption characteristics of aqueous extracts measured over the Southeastern United States. *Atmos. Chem. Phys.* 10, 5965–5977. doi:10.5194/acp-10-5965-2010

Hoffer, A., Gelencsér, A., Guyon, P., Kiss, G., Schmid, O., Frank, G., et al. (2006). Optical properties of humic-like substances (HULIS) in biomass-burning aerosols. *Atmos. Chem. Phys.* 6, 3563–3570. doi:10.5194/acp-6-3563-2006

Jiang, F., Song, J., Bauer, J., Gao, L., Vallon, M., Gebhardt, R., et al. (2022). Chromophores and chemical composition of brown carbon characterized at an urban kerbside by excitation–emission spectroscopy and mass spectrometry. *Atmos. Chem. Phys.* 22, 14971–14986. doi:10.5194/acp-22-14971-2022

Jiang, H., Li, J., Chen, D., Tang, J., Cheng, Z., Mo, Y., et al. (2020). Biomass burning organic aerosols significantly influence the light absorption properties of polarity-dependent organic compounds in the Pearl River Delta Region, China. *Environ. Int.* 144, 106079. doi:10.1016/j.envint.2020.106079

Jiang, H., Li, J., Sun, R., Tian, C., Tang, J., Jiang, B., et al. (2021). Molecular dynamics and light absorption properties of atmospheric dissolved organic matter. *Environ. Sci. Technol.* 55, 10268–10279. doi:10.1021/acs.est.1c01770

Jiang, H., Tang, J., Li, J., Zhao, S., Mo, Y., Tian, C., et al. (2022). Molecular signatures and sources of fluorescent components in atmospheric organic matter in SouthSouth China. *Environ. Sci. Technol. Lett.* 9, 913–920. doi:10.1021/acs.estlett.2c00629

Jung, J., Miyazaki, Y., Hur, J., Lee, Y. K., Jeon, M. H., Lee, Y., et al. (2023). Measurement report: summertime fluorescence characteristics of atmospheric water-soluble organic carbon in the marine boundary layer of the western Arctic Ocean. *Atmos. Chem. Phys.* 23, 4663–4684. doi:10.5194/acp-23-4663-2023

Kaskaoutis, D. G., Grivas, G., Oikonomou, K., Tavernaraki, P., Papoutsidaki, K., Tsagkaraki, M., et al. (2022). Impacts of severe residential wood burning on atmospheric processing, water-soluble organic aerosol and light absorption, in an inland city of Southeastern Europe. *Atmos. Environ.* 280, 119139. doi:10.1016/j.atmosenv.2022.119139

Kaskaoutis, D. G., Grivas, G., Theodosi, C., Tsagkaraki, M., Paraskevopoulou, D., Stavroulas, I., et al. (2020). Carbonaceous aerosols in contrasting atmospheric environments in Greek cities: evaluation of the EC-tracer methods for secondary organic carbon estimation. *Atmosphere* 11, 161. doi:10.3390/atmos11020161

Kaskaoutis, D. G., Petrinoli, K., Grivas, G., Kalkavouras, P., Tsagkaraki, M., Tavernaraki, K., et al. (2024). Impact of peri-urban forest fires on air quality and aerosol optical and chemical properties: the case of the August 2021 wildfires in Athens, Greece. *Sci. Total Environ.* 907, 168028. doi:10.1016/j.scitotenv.2023.168028

Ke, H., Gong, S., He, J., Zhou, C., Zhang, L., and Zhou, Y. (2019). Spatial and temporal distribution of open bio-mass burning in China from 2013 to 2017. *Atmos. Environ.* 210, 156–165. doi:10.1016/j.atmosenv.2019.04.039

Kroll, J. H., Donahue, N. M., Jimenez, J. L., Kessler, S. H., Canagaratna, M. R., Wilson, K. R., et al. (2011). Carbon oxidation state as a metric for describing the chemistry of atmospheric organic aerosol. *Nat. Chem.* 3, 133–139. doi:10.1038/nchem.948

Kuang, B. Y., Lin, P., Huang, X. H. H., and Yu, J. Z. (2015). Sources of humic-like substances in the Pearl River Delta, China: positive matrix factorization analysis of PM^{2.5} major components and source markers. *Atmos. Chem. Phys.* 15, 1995–2008. doi:10.5194/acp-15-1995-2015

Kunwar, B., and Kawamura, K. (2014). One-year observations of carbonaceous and nitrogenous components and major ions in the aerosols from subtropical Okinawa Island, an outflow region of Asian dusts. *Atmos. Chem. Phys.* 14, 1819–1836. doi:10.5194/acp-14-1819-2014

Laskin, A., Laskin, J., and Nizkorodov, S. A. (2015). Chemistry of atmospheric brown carbon. *Chem. Rev.* 115, 4335–4382. doi:10.1021/cr5006167

Lee, H. J., Laskin, A., Laskin, J., and Nizkorodov, S. A. (2013). Excitation-emission spectra and fluorescence quantum yields for fresh and aged biogenic secondary organic aerosols. *Environ. Sci. Technol.* 47, 5763–5770. doi:10.1021/es400644c

Li, B., Zhang, J., Zhao, Y., Yuan, S., Zhao, Q., Shen, G., et al. (2015). Seasonal variation of urban carbonaceous aerosols in a typical city Nanjing in Yangtze River Delta, China. *Atmos. Environ.* 106, 223–231. doi:10.1016/j.atmosenv.2015.01.064

Li, M., Fan, X., Zhu, M., Zou, C., Song, J., Wei, S., et al. (2018). Abundance and light absorption properties of Brown carbon emitted from residential coal combustion in China. *Environ. Sci. Technol.* 53, 595–603. doi:10.1021/acs.est.8b05630

Li, P., Yue, S., Yang, X., Liu, D., Zhang, Q., Hu, W., et al. (2023). Fluorescence properties and chemical composition of fine particles in the background atmosphere of north China. *Adv. Atmos. Sci.* 40, 1159–1174. doi:10.1007/s00376-022-2208-x

Lin, G., Penner, J. E., Flanner, M. G., Sillman, S., Xu, L., and Zhou, C. (2014). Radiative forcing of organic aerosol in the atmosphere and on snow: effects of SOA and brown carbon. *J. Geophys. Res.-Atmos.* 119, 7453–7476. doi:10.1002/2013JD021186

Liu, D., He, C., Schwarz, J. P., and Wang, X. (2020). Lifecycle of light-absorbing carbonaceous aerosols in the atmosphere. *npj Clim. Atmos. Sci.* 3, 40. doi:10.1038/s41612-020-00145-8

Liu, J., Bergin, M., Guo, H., King, L., Kotra, N., Edgerton, E., et al. (2013). Size-resolved measurements of brown carbon in water and methanol extracts and estimates of their contribution to ambient fine-particle light absorption. *Atmos. Chem. Phys.* 13, 12389–12404. doi:10.5194/acp-13-12389-2013

Liu, J., Mo, Y., Ding, P., Li, J., Shen, C., and Zhang, G. (2018). Dual carbon isotopes ((14)C and (13)C) and optical properties of WSOC and HULIS-C during winter in Guangzhou, China. *Sci. Total Environ.* 633, 1571–1578. doi:10.1016/j.scitotenv.2018.03.293

Liu, S., Aiken, A. C., Gorkowski, K., Dubey, M. K., Cappa, C. D., Williams, L. R., et al. (2015). Enhanced light absorption by mixed source black and brown carbon particles in UK winter. *Nat. Commun.* 6, 8435. doi:10.1038/ncomms9435

Liu, X., Wang, H., Wang, F., Lv, S., Wu, C., Zhao, Y., et al. (2023). Secondary Formation of atmospheric Brown carbon in China haze: implication for an enhancing role of ammonia. *Environ. Sci. Technol.* 57, 11163–11172. doi:10.1021/acs.est.3c03948

Lv, S., Gong, D., Ding, Y., Lin, Y., Wang, H., Ding, H., et al. (2019). Elevated levels of glyoxal and methylglyoxal at a remote mountain site in southern China: prompt *in-situ* formation combined with strong regional transport. *Sci. Total Environ.* 672, 869–882. doi:10.1016/j.scitotenv.2019.04.020

Lv, S., Wang, F., Wu, C., Chen, Y., Liu, S., Zhang, S., et al. (2022). Gas-to-Aerosol phase partitioning of atmospheric water-soluble organic compounds at a rural site in China: an enhancing effect of NH(3) on SOA formation. *Environ. Sci. Technol.* 56, 3915–3924. doi:10.1021/acs.est.1c06855

Ma, Y., Cheng, Y., Qiu, X., Cao, G., Kuang, B., Yu, J. Z., et al. (2019). Optical properties, source apportionment and redox activity of humic-like substances (HULIS) in airborne fine particulates in Hong Kong. *Environ. Pollut.* 255, 113087. doi:10.1016/j.envpol.2019.113087

Matos, J. T. V., Freire, S. M. S. C., Duarte, R. M. B. O., and Duarte, A. C. (2015). Natural organic matter in urban aerosols: comparison between water and alkaline soluble components using excitation–emission matrix fluorescence spectroscopy and multiway data analysis. *Atmos. Environ.* 102, 1–10. doi:10.1016/j.atmosenv.2014.11.042

Mo, Y., Li, J., Jiang, B., Su, T., Geng, X., Liu, J., et al. (2018). Sources, compositions, and optical properties of humic-like substances in Beijing during the 2014 APEC summit: results from dual carbon isotope and Fourier-transform ion cyclotron resonance mass spectrometry analyses. *Environ. Pollut.* 239, 322–331. doi:10.1016/j.envpol.2018.04.041

Mo, Y., Zhong, G., Li, J., Liu, X., Jiang, H., Tang, J., et al. (2022). The sources, molecular compositions, and light absorption properties of water-soluble organic carbon in marine aerosols from South China sea to the eastern Indian ocean. *J. Geophys. Res.-Atmos.* 127. doi:10.1029/2021jd036168

Mo, Y. Z., Li, J., Cheng, Z. N., Zhong, G. C., Zhu, S. Y., Tian, C. G., et al. (2021). Dual carbon isotope-based source apportionment and light absorption properties of water-soluble organic carbon in PM2.5 over China. *J. Geophys. Res.-Atmos.* 126. doi:10.1029/2020JD033920

Murphy, K. R., Stedmon, C. A., Graeber, D., and Bro, R. (2013). Fluorescence spectroscopy and multi-way techniques. PARAFAC. *PARAFAC. Anal. Methods* 5, 6557–6566. doi:10.1039/c3ay41160e

Niu, X., Pu, W., Fu, P., Chen, Y., Xing, Y., Wu, D., et al. (2022). Fluorescence characteristics, absorption properties, and radiative effects of water-soluble organic carbon in seasonal snow across northeastern China. *Atmos. Chem. Phys.* 22, 14075–14094. doi:10.5194/acp-22-14075-2022

Paraskevopoulou, D., Kaskaoutis, D. G., Grivas, G., Bikkina, S., Tsagkaraki, M., Vrettou, I. M., et al. (2023). Brown carbon absorption and radiative effects under intense residential wood burning conditions in Southeastern Europe: new insights into the abundance and absorptivity of methanol-soluble organic aerosols. *Sci. Total Environ.* 860, 160434. doi:10.1016/j.scitotenv.2022.160434

Park, S. S., and Yu, J. (2016). Chemical and light absorption properties of humic-like substances from biomass burning emissions under controlled combustion experiments. *Atmos. Environ.* 136, 114–122. doi:10.1016/j.atmosenv.2016.04.022

Petit, J. E., Favez, O., Albinet, A., and Canonaco, F. (2017). A user-friendly tool for comprehensive evaluation of the geographical origins of atmospheric pollution: wind and trajectory analyses. *Environ. Model. Softw.* 88, 183–187. doi:10.1016/j.envsoft.2016.11.022

Pio, C., Cerqueira, M., Harrison, R. M., Nunes, T., Mirante, F., Alves, C., et al. (2011). OC/EC ratio observations in Europe: Re-thinking the approach for apportionment between primary and secondary organic carbon. *Atmos. Environ.* 45, 6121–6132. doi:10.1016/j.atmosenv.2011.08.045

Pöschl, U. (2003). Aerosol particle analysis: challenges and progress. *Anal. Bioanal. Chem.* 375, 30–32. doi:10.1007/s00216-002-1611-5

Shen, Z., Zhang, Q., Cao, J., Zhang, L., Lei, Y., Huang, Y., et al. (2017). Optical properties and possible sources of brown carbon in PM2.5 over Xi'an, China. *Atmos. Environ.* 150, 322–330. doi:10.1016/j.atmosenv.2016.11.024

Shetty, N. J., Pandey, A., Baker, S., Hao, W. M., and Chakrabarty, R. K. (2019). Measuring light absorption by freshly emitted organic aerosols: optical artifacts in traditional solvent-extraction-based methods. *Atmos. Chem. Phys.* 19, 8817–8830. doi:10.5194/acp-19-8817-2019

Shiraiwa, M., Ueda, K., Pozzer, A., Lammel, G., Kampf, C. J., Fushimi, A., et al. (2017). Aerosol health effects from molecular to global scales. *Environ. Sci. Technol.* 51, 13545–13567. doi:10.1021/acs.est.7b04417

Simoneit, B. R. T. (2002). Biomass burning - a review of organic tracers for smoke from incomplete combustion. *Appl. Geochem.* 17, 129–162. doi:10.1016/s0883-2927(01)00061-0

Siu, C. L., Lee, L., Li, X. D., Zhang, G., Peng, X. Z., and Zhang, L. (2005). Biomonitoring of trace metals in the atmosphere using moss (*Hypnum plumaeforme*) in the nanling mountains and the Pearl River Delta, southern China. *Atmos. Environ.* 39, 397–407. doi:10.1016/j.atmosenv.2004.09.067

Srinivas, B., Rastogi, N., Sarin, M. M., Singh, A., and Singh, D. (2016). Mass absorption efficiency of light absorbing organic aerosols from source region of paddy-residue burning emissions in the Indo-Gangetic Plain. *Atmos. Environ.* 125, 360–370. doi:10.1016/j.atmosenv.2015.07.017

Srivastava, D., Favez, O., Perraudin, E., Villenave, E., and Albinet, A. (2018). Comparison of measurement-based methodologies to apportion secondary organic carbon (SOC) in PM2.5: a review of recent studies. *Atmosphere* 9, 452. doi:10.3390/atmos9110452

Sudheer, A. K., Aslam, M. Y., Upadhyay, M., Rengarajan, R., Bhushan, R., Rathore, J. S., et al. (2016). Carbonaceous aerosol over semi-arid region of western India: heterogeneity in sources and characteristics. *Atmos. Res.* 178-179, 268–278. doi:10.1016/j.atmosres.2016.03.026

Tan, J., Duan, J., Ma, Y., He, K., Cheng, Y., Deng, S.-x., et al. (2016). Long-term trends of chemical characteristics and sources of fine particle in Foshan City, Pearl River Delta: 2008–2014. *Sci. Total Environ.* 565, 519–528. doi:10.1016/j.scitotenv.2016.05.059

Tang, J., Li, J., Su, T., Han, Y., Mo, Y., Jiang, H., et al. (2020). Molecular compositions and optical properties of dissolved brown carbon in biomass burning, coal combustion, and vehicle emission aerosols illuminated by excitation–emission matrix spectroscopy and Fourier transform ion cyclotron resonance mass spectrometry analysis. *Atmos. Chem. Phys.* 20, 2513–2532. doi:10.5194/acp-20-2513-2020

Tang, J., Li, J., Zhao, S., Zhong, G., Mo, Y., Jiang, H., et al. (2024). Molecular signatures and formation mechanisms of water-soluble chromophores in particulate matter from Karachi in Pakistan. *Sci. Total Environ.* 914, 169890. doi:10.1016/j.scitotenv.2024.169890

Tang, J., Wang, J., Zhong, G., Jiang, H., Mo, Y., Zhang, B., et al. (2021). Measurement report: long-emission-wavelength chromophores dominate the light absorption of brown carbon in aerosols over Bangkok: impact from biomass burning. *Atmos. Chem. Phys.* 21, 11337–11352. doi:10.5194/acp-21-11337-2021

Tao, J., Zhang, L., Cao, J., and Zhang, R. (2017). A review of current knowledge concerning PM_{2. 5} chemical composition, aerosol optical properties and their relationships across China. *Atmos. Chem. Phys.* 17, 9485–9518. doi:10.5194/acp-17-9485-2017

Teich, M., van Pinxteren, D., Wang, M., Kecorius, S., Wang, Z., Müller, T., et al. (2017). Contributions of nitrated aromatic compounds to the light absorption of water-soluble and particulate brown carbon in different atmospheric environments in Germany and China. *Atmos. Chem. Phys.* 17, 1653–1672. doi:10.5194/acp-17-1653-2017

Tian, J., Wang, Q., Ni, H., Wang, M., Zhou, Y., Han, Y., et al. (2019). Emission characteristics of primary Brown carbon absorption from biomass and coal burning: development of an optical emission inventory for China. *J. Geophys. Res.-Atmos.* 124, 1879–1893. doi:10.1029/2018JD029352

Tiwari, S., Kaskaoutis, D., Soni, V. K., Dev Attri, S., and Singh, A. K. (2018). Aerosol columnar characteristics and their heterogeneous nature over Varanasi, in the central Ganges valley. *Environ. Sci. Pollut. Res. Int.* 25, 24726–24745. doi:10.1007/s11356-018-2502-4

Wang, J., Jiang, H., Jiang, H., Mo, Y., Geng, X., Li, J., et al. (2020). Source apportionment of water-soluble oxidative potential in ambient total suspended particulate from Bangkok: biomass burning versus fossil fuel combustion. *Atmos. Environ.* 235, 117624. doi:10.1016/j.atmosenv.2020.117624

Wang, Q., Han, Y., Ye, J., Liu, S., Pongpiachan, S., Zhang, N., et al. (2019). High contribution of secondary Brown carbon to aerosol light absorption in the southeastern margin of Tibetan plateau. *Geophys. Res. Lett.* 46, 4962–4970. doi:10.1029/2019gl082731

Wang, Q., Zhou, Y., Ma, N., Zhu, Y., Zhao, X., Zhu, S., et al. (2022). Review of Brown carbon aerosols in China: pollution level, optical properties, and emissions. *J. Geophys. Res.-Atmos.* 127. doi:10.1029/2021jd035473

Wang, X., Heald, C. L., Liu, J., Weber, R. J., Campuzano-Jost, P., Jimenez, J. L., et al. (2018). Exploring the observational constraints on the simulation of brown carbon. *Atmos. Chem. Phys.* 18, 635–653. doi:10.5194/acp-18-635-2018

Wong, J. P. S., Tsagkaraki, M., Tsiodra, I., Mihalopoulos, N., Violaki, K., Kanakidou, M., et al. (2019). Atmospheric evolution of molecular-weight-separated brown carbon from biomass burning. *Atmos. Chem. Phys.* 19, 7319–7334. doi:10.5194/acp-19-7319-2019

Wu, C., and Yu, J. Z. (2016). Determination of primary combustion source organic carbon-to-elemental carbon (OC/EC) ratio using ambient OC and EC measurements: secondary OC-EC correlation minimization method. *Atmos. Chem. Phys.* 16, 5453–5465. doi:10.5194/acp-16-5453-2016

Wu, G., Fu, P., Ram, K., Song, J., Chen, Q., Kawamura, K., et al. (2021). Fluorescence characteristics of water-soluble organic carbon in atmospheric aerosol. *Environ. Pollut.* 268, 115906. doi:10.1016/j.envpol.2020.115906

Wu, G., Ram, K., Fu, P., Wang, W., Zhang, Y., Liu, X., et al. (2019). Water-soluble Brown carbon in atmospheric aerosols from Godavari (Nepal), a regional representative of South Asia. *Environ. Sci. Technol.* 53, 3471–3479. doi:10.1021/acs.est.9b00596

Wu, G., Wan, X., Ram, K., Li, P., Liu, B., Yin, Y., et al. (2020). Light absorption, fluorescence properties and sources of brown carbon aerosols in the Southeast Tibetan Plateau. *Environ. Pollut.* 257, 113616. doi:10.1016/j.envpol.2019.113616

Xiong, R., Li, J., Zhang, Y., Zhang, L., Jiang, K., Zheng, H., et al. (2022). Global brown carbon emissions from combustion sources. *Env. Sci. Ecotechnol.* 12, 100201. doi:10.1016/j.ese.2022.100201

Xu, J., Hettiyadura, A. P. S., Liu, Y., Zhang, X., Kang, S., and Laskin, A. (2020). Regional differences of chemical composition and optical properties of aerosols in the Tibetan plateau. *J. Geophys. Res.-Atmos.* 125, e2019JD031226. doi:10.1029/2019jd031226

Xu, J. Z., Zhang, Q., Wang, Z. B., Yu, G. M., Ge, X. L., and Qin, X. (2015). Chemical composition and size distribution of summertime PM_{2.5} at a high altitude remote location in the northeast of the Qinghai–Xizang (Tibet) Plateau: insights into aerosol sources and processing in free troposphere. *Atmos. Chem. Phys.* 15, 5069–5081. doi:10.5194/acp-15-5069-2015

Xu, L., Wu, X., Hong, Z., Zhang, Y., Deng, J., Hong, Y., et al. (2019). Composition, mixing state, and size distribution of single submicron particles during pollution episodes in a coastal city in southeast China. *Environ. Sci. Pollut. Res. Int.* 26, 1464–1473. doi:10.1007/s11356-018-3469-x

Yan, C., Zheng, M., Bosch, C., Andersson, A., Desyaterik, Y., Sullivan, A. P., et al. (2017). Important fossil source contribution to brown carbon in Beijing during winter. *Sci. Rep.* 7, 43182. doi:10.1038/srep43182

Yan, C., Zheng, M., Sullivan, A. P., Bosch, C., Desyaterik, Y., Andersson, A., et al. (2015). Chemical characteristics and light-absorbing property of water-soluble organic carbon in Beijing: Biomass burning contributions. *Atmos. Environ.* 121, 4–12. doi:10.1016/j.atmosenv.2015.05.005

Yin, X., Huang, Z., Zheng, J., Yuan, Z., Zhu, W., Huang, X., et al. (2017). Source contributions to PM2.5 in Guangdong province, China by numerical modeling: results and implications. *Atmos. Res.* 186, 63–71. doi:10.1016/j.atmosres.2016.11.007

Yuan, W., Huang, R. J., Yang, L., Guo, J., Chen, Z., Duan, J., et al. (2020). Characterization of the light-absorbing properties, chromophore composition and sources of brown carbon aerosol in Xi'an, northwestern China. *Atmos. Chem. Phys.* 20, 5129–5144. doi:10.5194/acp-20-5129-2020

Yue, S., Bikkina, S., Gao, M., Barrie, L. A., Kawamura, K., and Fu, P. (2019). Sources and radiative absorption of water-soluble Brown carbon in the high arctic atmosphere. *Geophys. Res. Lett.* 46, 14881–14891. doi:10.1029/2019GL085318

Zeng, L., Zhang, A., Wang, Y., Wagner, N. L., Katich, J. M., Schwarz, J. P., et al. (2020). Global measurements of Brown carbon and estimated direct radiative effects. *Geophys Res. Lett.* 47, e2020GL088747. doi:10.1029/2020GL088747

Zhang, C., Chen, M., Kang, S., Yan, F., Han, X., Gautam, S., et al. (2021). Light absorption and fluorescence characteristics of water-soluble organic compounds in carbonaceous particles at a typical remote site in the southeastern Himalayas and Tibetan Plateau. *Environ. Pollut.* 272, 116000. doi:10.1016/j.envpol.2020.116000

Zhang, L. Y., Son, J. H., Bai, Z., Zhang, W., Li, L., Wang, L. N., et al. (2022). Characterizing atmospheric Brown carbon and its emission sources during wintertime in Shanghai, China. *Atmosphere* 13, 991. doi:10.3390/atmos13060991

Zhang, Q., Shen, Z., Zhang, L., Zeng, Y., Ning, Z., Zhang, T., et al. (2020). Investigation of primary and secondary particulate Brown carbon in two Chinese cities of xi'an and Hong Kong in wintertime. *Environ. Sci. Technol.* 54, 3803–3813. doi:10.1021/acs.est.9b05332

Zhang, X., Lin, Y. H., Surratt, J. D., and Weber, R. J. (2013). Sources, composition and absorption Angstrom exponent of light-absorbing organic components in aerosol extracts from the Los Angeles Basin. *Environ. Sci. Technol.* 47, 3685–3693. doi:10.1021/es305047b

Zhao, Y., Wu, C., Wang, Y.-Q., Chen, Y.-B., Lu, S.-J., Wang, F.-L., et al. (2021). Pollution characteristics and sources of wintertime atmospheric Brown carbon at a background site of the Yangtze River Delta region in China. *Huan jing ke xue= Huanjing kexue* 42, 3127–3135. doi:10.13227/j.hjkx.202012002

Zou, C., Cao, T., Li, M., Song, J., Jiang, B., Jia, W., et al. (2023). Measurement report: changes in light absorption and molecular composition of water-soluble humic-like substances during a winter haze bloom-decay process in Guangzhou, China. *Atmos. Chem. Phys.* 23, 963–979. doi:10.5194/acp-23-963-2023